STUDYING THE EFFECTS OF WAG PARAMETERS ON CO_2 FLOODING RECOVERY EFFICIENCY

A Thesis in partial fulfillment of the requirments for the degree of

Master of Science in Petroleum Engineering

Submitted to the Department of Mineral Resources and Petroleum Engineering,
Chair of Reservoir Engineering

MONTAN UNIVERSITÄT

By

Nidal Bashir Khalef, BSc

Under supervision of

Univ.-Prof. Dipl. Geol. PhD Stephan K. Matthäi

December 2009

AFFIDAVIT

I declare in lieu of oath, that I wrote this thesis and performed the associated research myself, using only literature cited in this volume.

_____ _____

Datum Unterschrift

KURZFASSUNG

Das Mobilitaetsverhaeltnis, welches die Verdraengung von Oel durch Gas waehrend einer Gasinjektion kennzeichnet, ist aufgrund der niedrigen Viskositaet von Gas typischerweise unvorteilhaft. Dieses Problem macht Mobilitaet und Flutprofilkontrolle zu den wichtigsten Einflussfaktoren fuer erfolgreiche CO_2-Flutungen. Um das Flutprofil zu kontrollieren, wurde der "Water-Alternating-Gas"-Prozess (WAG-Prozess) entwickelt. Die hoehere mikroskopische Verdraengungseffizienz von Gas in Verbindung mit der hoeheren makroskopischen Verdraengungseffizienz von Wasser erhoehen die zusaetzliche Oelausbeute signifikant im Vergleich zu Wasserflutungen. Als wichtige technische Faktoren, welche das Ergebnis eines WAG-Prozesses beeinflussen, konnten folgende Faktoren identifiziert werden: Heterogeneitaet, Geometrie des Flusses, Benetzbarkeit, Mischungskonditionen, Injektionstechniken und WAG-Parameter.

Meine MSc-Forschungen haben sich darauf konzentriert, den Effekt des WAG-Verhaeltnisses, der CO_2-Slug-Groesse und der CO_2-Injektionsrate auf die Ausbeuteeffizienz in heterogenen Systemen zu bestimmen. Ich habe die Ausbeuteeffizienzen in einer Serie von Simulation Runs in einem kompositionellen Simulator, welcher die Peng-Robinson- Zustandsgleichung verwendet, verglichen. Diese Sensitivitaetsvergleiche wurden mit vier verschiedenen WAG-Verhaeltnissen, vier CO_2-Slug-Groessen und vier Injektionsraten durchgefuehrt. Als heterogenes System wurde ein "Upscaled SPE 10 comparative solution project model" verwendet.
Meine Ergebnisse zeigen, dass die erzielte Ausbeute unter Verwendung eines WAG-Prozesses eine Funktion der Injektionsrate, des WAG-Verhaeltnisses und der CO_2-Slug-Groesse ist. Diese Parameter kontrollieren die endgueltige raeumliche Oelverteilung und die Verdraengungsfront fuer die Permeabilitaetsstruktur der Lagerstaette. Je groesser die CO_2-Slug-Groesse ist, desto groesser ist die kumulative Oelausbeute, aber ab einem bestimmten Kennwert (optimale Slug-Groesse) wird die zusaetzliche Ausbeute immer kleiner und wird in manchen Faellen sogar negativ. Der

beste kumulative Ausbeutegrad wird bei einem WAG-Verhaeltnis von 2:1 erreicht. Wenn die Slug-Groesse und das WAG-Verhaeltnis gleich sind, verringert eine Erhoehung der Injektionsrate die finale Oelausbeute. Die kumulative Oelausbeute durch kontinuierliches Fluten mit CO_2 war in manchen Faellen 29% niedriger im Vergleich zum WAG-Schema. Meine wissenschaftliche Arbeit zeigt, dass es ohne Simulation nicht moeglich ist, einen WAG-Prozess fuer ein heterogenes System zu planen und zu optimieren.

ABSTRACT

The mobility ratio, which controls the sweep between the injected gas and the displaced oil bank in a gas injection process, is typically highly unfavorable due to the relatively low viscosity of the injected CO_2. This difference makes mobility and consequently flood profile control the biggest concerns for the successful application of CO_2 flooding. This led to the development of the Water-Alternating-Gas (WAG) process as a means of controlling the flood profile. The higher microscopic displacement efficiency of gas combined with the better macroscopic sweep efficiency of water significantly increases the incremental oil production as compared with waterflooding. Important technical factors affecting WAG performance that have been identified are heterogeneity, flow geometry wettability, miscibility conditions, injection techniques, and WAG parameters.

My MSc research has aimed at studying the effect of the WAG ratio, CO_2 slug size, and CO_2 injection rate on oil recovery efficiency in heterogeneous system. I compared the recovery efficiency observed in a series of simulation runs using a compositional simulator with the Peng-Robinson equation of state (EOS).These sensitivity runs were performed by assuming four WAG ratios, four CO_2 slug sizes, and four injection rates. An upscaled SPE 10 comparative solution project model was selected for the compositional simulation as a heterogeneous system. My results indicate that the recovery obtained using the WAG process is a function of the injection rate as well as the WAG ratio and the CO_2 slug size. These control the final spatial oil distribution and the displacement front given the permeability structure of the reservoir. The larger the CO_2 slug size the greater the cumulative oil recovery, but at a certain value (optimum slug size) the incremental improvement of recovery gets smaller and smaller and in some cases recovery even decreases. The highest cumulative recovery is obtained at a WAG ratio of 2:1. At the same slug size and WAG ratio, increasing the CO2 injection rate decreases total oil recovery. The cumulative oil recovery obtained by continuous CO_2 flooding was in some cases 29 % low comparing to the WAG scheme. My research shows that without simulation it is not possible to predict and optimize WAG for a heterogeneous system.

DEDICATION

This work is dedicated to
my parents, son, daughter, and wife.

ACKNOWLEDGMENTS

I wish to express my gratitude to my thesis advisor Prof. Dr Stephan k. Matthäi for his patience and understanding, his guidance, advice, encouragement and moral support throughout this work.

I wish to express my gratitude to the OMV Libya for sponsoring my study in Montan University.

I would like to thank and express my deepest appreciation to all my friends and colleagues in the Reservoir Engineering Department for all their support.

I would like to extend my appreciation to the employees of the department of mineral resources and petroleum engineering at Montan University for their constant encouragement and support.

Last but not least, special and infinite thanks to the most important people in my life, my parents, my children, and my wife, all of your love, respect, encouragement and support.

TABLE OF CONTENTS

LIST OF TABLES

LIST OF FIGURES

CHAPTER 1 INTRODUCTION

1.1 Background

The means by which CO_2 increase oil recovery includes oil swelling, the reduction of the viscosity, the reduction of oil density, the extraction or vaporization of oil, the reduction of interfacial tension, solution CO_2 gas drive, increase in injectivity, the acidizing of carbon formation and the miscibility effects.

The mobility ratio, which controls the volumetric sweep, between the injected gas and displaced oil bank in gas processes, is typically highly unfavorable due to the relatively low viscosity of the injected phase. This difference makes mobility and consequently flood profile control the biggest concerns for the successful application of this process.

These concerns led to the development of the Water-Alternating-Gas (WAG) process for flood profile control.

WAG injection is a combining of two traditional technologies - waterflooding and gas injection. The WAG injection was originally proposed as a method to improve sweep of gas injection, mainly by using the water to control the mobility of the displacement and to stabilize the front. Because the microscopic displacement of the oil by gas is normally better than by water, the WAG injection combines the improved displacement efficiency of the gas flooding with an improved macroscopic sweep by water injection.

The first field application of WAG is attributed to the North Pembina field in Alberta, Canada by Mobil in 1957.[1] Reservoir heterogeneity has a strong influence on the gas/oil displacement process.

The main factors affecting the WAG injection process in addition to are the reservoir heterogeneity (stratification and anisotropy) are rock wettability, fluid properties, miscibility conditions, gas trapped, injection technique and WAG parameters as cycling frequency, slug size, WAG ratio, injection rate.[6]

1.2 Objective

This research is directed towards the study of the effect of WAG parameters on oil recovery efficiency by CO_2 in relatively heterogeneous upscaled SPE 10 model and compares the recovery efficiency from series simulation runs using ECLIPSE 300 compositional simulator with Peng-Robinson equation of state (EOS).

1.3 Method

In order to accomplish the proposed objectives, various sensitivity runs were performed by assuming four WAG ratios, four CO_2 slug sizes, and four injection rates. A series of WAG ratio and CO_2 slug sizes sensitivities were compared. Water alternating with CO_2 injections at four different WAG ratios (2:1, 1.25:1, 1:1, and 0.5:1) was performed. The runs evaluated total CO_2 slug sizes at 5, 10, 12.5 and 15% HCPV. WAG processes used two HCPV increments of CO_2 slug. After injection of each CO_2 increment, injection was switched to water until its increment volume was complete. Alternate injection of the two fluids was continued until the total desired CO_2 slug volume had been injected. Water and CO_2 were injected at rate of 5000 BBL/D and 3000 Mscf /D, respectively. The producers are constrained by bottom-hole pressure and operated with a minimum constraint value of 40000 psi as a lower limit. (Calculation procedure is shown in Appendix D).

To investigate the effect of the CO_2 injection rate on the WAG process four sensitivities were performed at a WAG ratio of 1:1 for 12.5% HCPV of slug size with constant rates of 5000 res BBL/D of water and 2000, 3000, 4000 and 5000 Mscf /D of CO_2. Oil recoveries and production performance were monitored and compared for these runs.

For additional comparison, continues CO_2 injection is ccompared at WAG ratio of 1:1 and 15% slug size.

CHAPTER 2 LITERATURE REVIEW

A comprehensive review of the literature on the WAG process is presented in this section.

2.1 Description and Mechanisms of Carbon Dioxide Flooding

Gas injection is certainly one of the oldest methods utilized by engineers to improve recovery, and its use has increased recently, although most of the new expansion has been coming from the non-hydrocarbon gases. Because of the increasing interest in CO_2 and nitrogen or flue gas methods, they are separated from the hydrocarbon miscible techniques

CO_2 is effective for recovery of oil for a number of reasons. In general, carbon dioxide is very soluble in crude oils at reservoir pressures; therefore, it swells the net volume of oil and reduces its viscosity even before miscibility is achieved by the vaporizing gas drive mechanism.

Although the mechanism for CO_2 flooding appears to be the same as that for hydrocarbon miscible floods, CO_2 floods may give better recoveries even if both systems are above their required miscibility pressures, especially in tertiary floods. Compared to hydrocarbons, CO_2 has a much higher solubility in water, and it has been observed in laboratory experiments to diffuse through the water phase to swell bypassed oil until the oil is mobile. Thus, not only are the oil and depth screening criteria easier to meet in CO_2 flooding, but the ultimate recovery may be better than with hydrocarbons when above the MMP. [2]

Carbon dioxide flooding is carried out by injecting quantities of CO_2 into the reservoir. Although CO_2 is not truly miscible with the crude oil, the CO_2 extracts the light-to-intermediate components from the oil, and, if the pressure is high enough, develops miscibility to displace the crude oil from the reservoir. CO_2 recovers crude oil also by swelling the crude oil and lowering the viscosity of the oil.

2.2 Mobility Control Process

The oil recovery, R_f, can be described by three contributions;

$$R_f = E_v \times E_h \times E_m \quad \text{..... (1)}$$

Where: E_v =vertical sweep, E_h = horizontal sweep, and E_m = microscopic displacement efficiency. The recovery can be optimized by maximizing any or all of the three factors.

The horizontal displacement efficiency (E_h) will be strongly influenced by the stability of the front that is defined by the mobility of the fluids. The mobility ratio (M) can be described as:

$$M = \frac{K_{rg} / \mu_g}{K_{ro} / \mu_o} \quad \text{.....(2)}$$

Where: K_{rg} and K_{ro} are the relative permeabilities and μ_g and μ_o are the viscosities for gas and oil, respectively. If an unfavorable mobility ratio is obtained, the gas will finger (or channel). This cause early gas breakthrough and decreases the sweep efficiency. Reports of these problems are given from several of the field cases.[1]

The displacement will be optimized if the mobility ratio is favorable (<1). Reduction of the mobility ratio can be obtained by increasing the gas viscosity or reducing the relative permeability of the fluids. Reduced mobility of the gas phase can be achieved by injecting water and gas alternately. Furthermore, the mobility is expected to be reduced when compared to gas injection.[1]

2.3 WAG Process

Water alternated gas (WAG) injection is a combining of two traditional technologies - waterflooding and gas injection. The WAG injection was originally proposed as a method to improve sweep of gas injection, mainly by using the water to control the mobility of the displacement and to stabilize the front. Because the microscopic displacement of the oil by gas is normally better than by water, the WAG injection combines the improved displacement efficiency of the gas flooding with an improved

macroscopic sweep by water injection. This has resulted in improved recovery compared to a pure water injection. It also improves the economics by reducing the volume of gas that needs to be injected into the reservoir.

The first field application of WAG is attributed to the North Pembina field in Alberta, Canada by Mobil in 1957.[1]

Conventional gas or waterflood usually leave at least 20–50% of the oil as residual. Laboratory models conducted early in the history of flooding showed that simultaneous water/ gas injection could have sweep efficiency as high as 90% for a five-spot flooding system. With gas alone the sweep out efficiency could only be about 60%. However, completion costs and the additional complexity in operations, as well as technical factors of gravity segregation, indicated that simultaneous water/gas injection was a difficult if not an impractical method to minimize mobility instabilities associated with gas flood process. Therefore the use of a slug followed by WAG has been adopted.[3]

The method finds larger and larger application and its control and efficiency improvement is an acute problem.[4]

In recent years there has been an increasing interest in water alternating- gas processes, both miscible and immiscible. The WAG process is shown schematically in Figure 1.

Gas injection projects contribute about 40% of the total US-EOR production: most of which are WAG floods. Almost 80% of the WAG flood projects in the US are reported an economic success.[5]

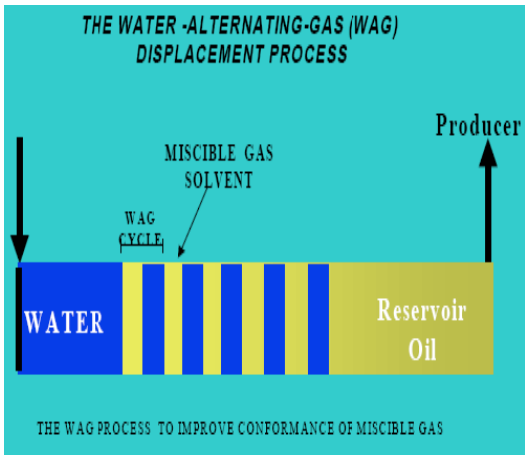

Figure 1: Schematic of the Water-Alternating-Gas Process. [6]

Initial studies indicate that CO_2 flooding would increase the ultimate recovery by about 8 to 14% of OOIP. However, the more recent survey of 2001 by Christensen et al.[1] shows that the average increase in oil recovery was only 5 – 10%. The survey encompassed 59 projects. The popularity of the WAG process is evident from the increasing number of projects and many successful field wide applications.

The survey as shown in Figure 2 also included the application scenario and distribution of the WAG process. US had the largest share of WAG applications followed by Canada. The process was seen mostly applied to onshore reservoirs (88%), but applicable to a wide range of reservoir types, from chalk to fine sandstone. The popularity of the miscible flood was evident from the fact that 79% of the WAG projects employed are miscible.

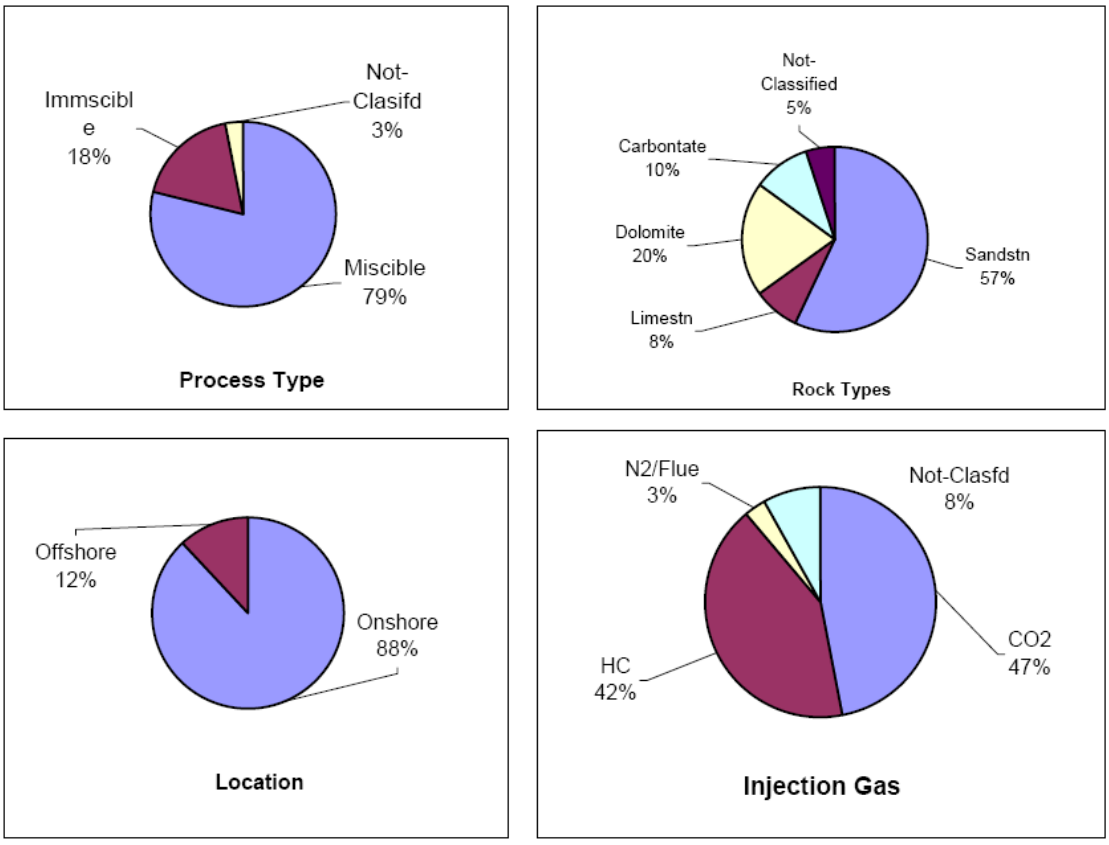

Figure 2: WAG survey – Distribution / Application of WAG. [1]

Expected incremental oil recoveries due to WAG-flooding, over waterflooding, in some of the projects presented in the literature are: 10-15% in the Permian Basin

miscible CO_2 injection projects, about 7% at Rangely miscible CO_2 injection project, and about 7% at lower Statfjord field by down-dip miscible hydrocarbon gas injection. Immiscible WAG-injection in some of the North Sea reservoirs is expected to yield 6-12% incremental oil recovery, over waterflood or gas injection.[6]

2.4 WAG Process Classification

Christensen et al. [1] have tried to classify the WAG process. They grouped the process into four types: Miscible, Immiscible, and others based on injection pressures and method of injection. Many reservoir specific processes developed have been patented and are generally grouped under the 'other' WAG classification. Some of the examples are the 'Hybrid-WAG' process patented by UNOCAL, and the Denver Unit WAG 'DUWAG' process of Shell.[7]

These patented processes namely; Hybrid-WAG and DUWAG were developed to optimize recoveries from gas injection processes wherein a large slug of CO_2 is injected followed by 1:1 WAG.

2.5 Design Parameters for the WAG Process

The WAG survey conducted by Christensen demonstrated that this process has been applied to rocks from very low permeability chalk up to high permeability sandstone. Most of the applied processes were miscible.[1] One of the first issues to decide is whether a miscible or immiscible drive should be applied. This decision is based on availability, but it is mainly reported to be an economic consideration. Several of the reviewed fields have been under re pressurization to achieve miscibility before WAG injection has been initiated. The main factors affecting the WAG injection process are the reservoir heterogeneity (stratification and anisotropy), rock wettability, fluid properties, miscibility conditions, gas trapped, injection technique and WAG parameters as cycling frequency, slug size, WAG ratio, injection rate.[6]

2.5.1 Reservoir Heterogeneity and Stratification

Stratification may strongly influence the water/gas displacement process. [6]
Horizontal fluid flow in vertically communicating porous strata are influenced by flow perpendicular to the bulk flow caused by viscosity forces, capillarity forces, gravity forces, and dispersion.[3] Usually, gas is found to give early breakthrough; this is caused not only by mobility ratio but also by the reservoir heterogeneity and especially high permeable layers.[1]

As with any kind of fluid displacement process, large variations in the permeability of a reservoir cause poor coverage by the injected fluids. This problem can be disastrous to a miscible flood process. Where there is crossflow between the zones of differing permeability, transverse dispersion causes early deterioration of the small slug and loss of miscibility. In those cases where there is no crossflow between zones, high-permeability zones tend to take a disproportionately large portion of the total slug injected. This leaves insufficient slug material to displace the oil in the less permeable zones and causes early loss of miscibility in these zones. At the least, reservoirs having extensive fractures or high permeability contrasts are poor risks for miscible displacement processes.[8]
The results show that vertical distribution of CO_2 is dominated by permeability contrasts, flow into each layer is essentiality proportional to the fraction of the overall system KH and almost independent of WAG ratio. [9]
The ratio of viscous to gravity forces is the prime variable for determining the efficiency of WAG injection and controls vertical conformance and displacement efficiency of the flood. Cross-flow or convective mixing can substantially increase injectivity even in the presence of low vertical to horizontal permeability ratios.
Cross-flow is more commonly existed in WAG projects. In this case generally the oil recovery is low due to the gravity segregation, Figure 3. As CO_2 flows preferentially toward the top portion of thick, high permeability zone, injected water may flow preferentially toward the lower portion of the zone.

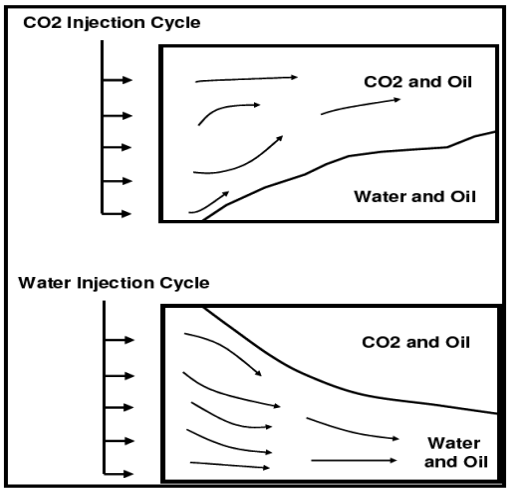

Figure 3: Gravity effect during WAG.

As shown in Figure 4, in highly stratified reservoirs, the higher permeability layer(s) always respond first, resulting in an early breakthrough and poor sweep efficiency.

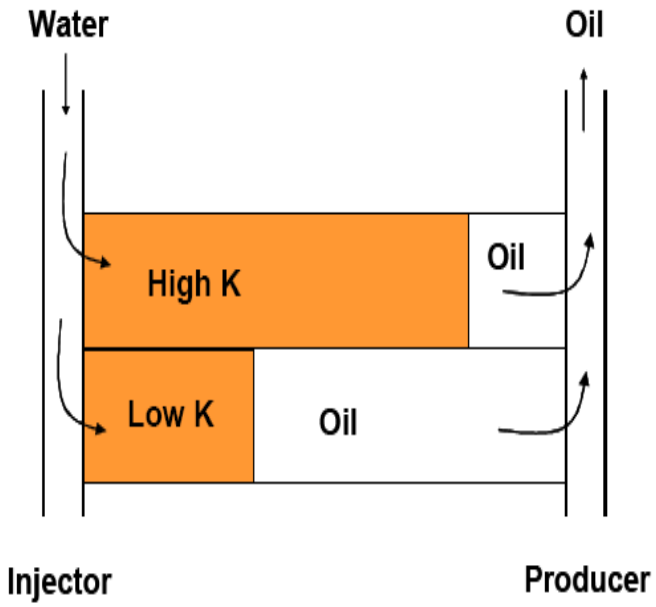

Figure 4: Displacement of oil by water in a stratified reservoir.

2.5.2 Relative permeability

2.5.2.1 Two-phase relative permeability

Because direct measurement of three-phase relative permeabilities is costly and very time consuming, it is standard practice to rely on two-phase relative permeability experimental data, and use an interpolation model to evaluate the relative permeabilities under three-phase flow conditions.

The most common models estimate relative permeability of oil, water, and gas under three-phase conditions by interpolation of two-phase data.

It is essential that the two-phase experiments reproduce a similar saturation history to that of the three-phase scenario to be estimated. In the WAG process, three distinct displacements take place, Figure 5: (1) imbibition from natural or man- made water drive, (2) gas food into water and residual oil, and (3) waterflood into gas and residual oil. It is apparent that relative permeabilities along saturation path (3) and subsequent gas and water injection are less likely to be well represented by the two-phase experimental curves.[10]

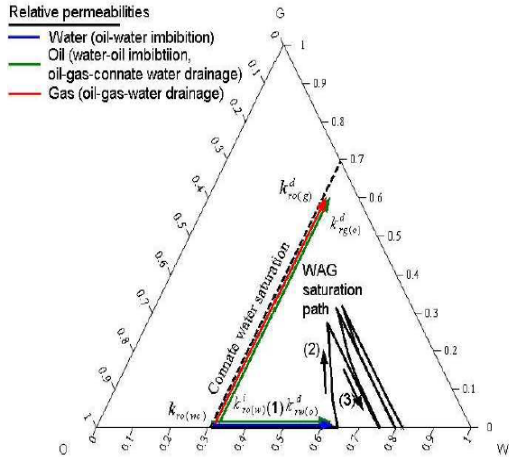

Figure 5: Typical saturation path in a WAG displacement process.[10]

From the two-phase input data, relative permeabilities are commonly estimated assuming: (1) water relative permeability is a function of water saturation only, (2) gas relative permeability is also a function of gas saturation only, and (3) oil relative permeability is a function of all three saturations.

The water relative permeability is typically obtained from an oil-water imbibition or drainage experiment. For strongly water-wet rocks, the choice is not critical because the water relative permeabilities are almost the same.

The gas relative permeability would be measured in an oil-gas experiment at connate water saturation. As opposed to water, gas relative permeability is a strong function of saturation history.

Because oil relative permeability is regarded as dependent upon all saturations, one must enter two experimental curves: the imbibition water-oil experiment, $k_{ro(w)}$, and a drainage gas-oil experiment at connate water, $k_{ro(g)}$.[10]

2.5.2.2 Three -phase interpolation models for oil relative permeability

The oil relative permeabilities from the two-phase experiments are then used to determine oil relative permeabilities in three-phase systems. Because oil relative permeability is a function of all three fluid saturations, an interpolation model is used to predict the relative permeability in the three-phase region between the oil-water and gas-oil-connate water saturation paths.

The most commonly-used interpolation models in reservoir simulators are Stone I, Stone II, and saturation weighted interpolation.[10]

In ECLIPSE , a choice of four different formulae (default model, Stone's first model, (Modified), Stone's second model (Modified), IKU method) are available for calculating the 3-phase oil relative permeability at particular water and gas saturations, from the input relative permeabilities of oil in water and oil in gas and connate water.

The default model for the 3-phase oil relative permeability provides a simple but effective formula which avoids the problems associated with other methods (poor conditioning, negative values etc.).

The default model (saturation weighted interpolation model) assumed by ECLIPSE computes the oil relative permeability as:

$$K_{ro} = \frac{S_g \times K^d{}_{ro(g)} + \left(S_w - S_{wc}\right) \times K^i{}_{ro(w)}}{S_g + S_w - S_{wc}} \quad \text{..... (3)}$$

Where S_g is the gas saturation, $K^d{}_{ro(g)}$ is the oil relative permeability for a system with oil, gas at connate water estimated from drainage gas- oil experiment at connate water

and (tabulated as a function of S_o), S_w is the oil saturation, S_{wc} is the connate water saturation, and $K^i_{ro(w)}$ is the imbibition oil relative permeability for a system with oil and water only estimated from imbibition water-oil experiment at connate water and (tabulated as a function of S_o).[11]

2.5.2.3 Relative permeability hysteresis in the non-wetting phase

Hysteresis refers to irreversibility, or path dependence. In multiphase flow, it manifests itself through the dependence of the relative permeabilities and capillary pressures on the saturation path and the saturation history. From the point of view of pore-scale processes, hysteresis has at least two sources. (1) The first source is trapping of the non-wetting phase: during an imbibition process, a fraction of the non-wetting phase gets disconnected in the form of blobs or ganglia, becoming effectively immobile (trapped). Hysteresis effects are larger in processes with strong flow reversals. This is the case of cyclic water and gas injection in a porous medium, in which the gas phase is trapped during water injection after a gas flood. (2) The second source is contact angle hysteresis: the advancing contact angle (of wetting phase displacing a non-wetting phase) is larger than the receding contact angle (of wetting phase retreating by non-wetting phase invasion) due to chemical heterogeneities or surface roughness.[10]

A typical pair of relative permeability curves for a non-wetting phase is shown in Figure 6. The curve 1 to 2 represents the user-supplied drainage relative permeability table, and the curve 2 to 3 represents the user-supplied imbibition relative permeability table. (Note that non-wetting phase saturation increases from right to left in this diagram). The critical saturation of the imbibition curve (S_{ncri}) is greater than that of the drainage curve (S_{ncrd}). The two curves must meet at the maximum saturation value (S_{nmax}).

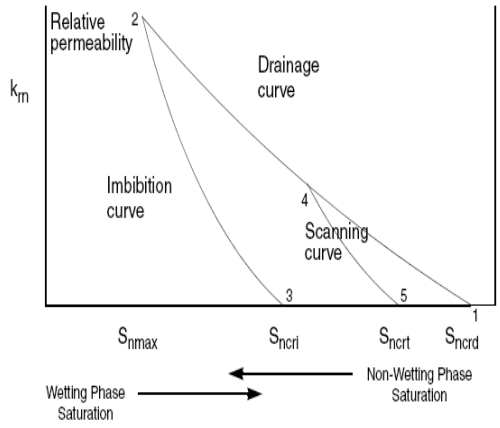

Figure 6: A typical pair of relative permeability curves for a non-wetting phase.[11]

If the drainage or imbibition process is reversed at some point, the data used does not simply run back over its previous values but runs along a scanning curve.

Consider a drainage process starting at point 1. If a full drainage process is carried out, the bounding drainage curve is followed to point 2. If an imbibition process then occurs, the water saturation increasing, the bounding imbibition curve is followed to point 3, the imbibition critical saturation.

But suppose that the drainage process is reversed at some intermediate point 4. A scanning curve results (curve 4 to 5 in the diagram). The critical saturation remaining at point 5 is the trapped critical saturation (S_{ncrt}) which is a function of the maximum non-wetting phase saturation reached in the run (S_{hy}).

If a further drainage process begins from any point on the scanning curve 5 to 4, the same scanning curve is retraced until (S_{hy}) is reached, at which point the drainage curve is rejoined. (S_{hy}) is updated during the run, so that further imbibition processes would occur along the appropriate scanning curves.

There is a choice of three methods for the generation of scanning curves from a given value of using Carlson's method or Killough's method or J. Jargon's method.[11]

A relative permeability hysteresis model characterizes the scanning curves during imbibition and drainage cycles.

Killough used Land's trapping model to derive a relative permeability hysteresis model as interpolative scheme for defining the intermediate scanning curves, intermediate

imbibition relative permeability curves between the bounding drainage $K^{d}_{rg(o)}$ and imbibition $K^{i}_{rg(o)}$ relative permeability curves, Figure 7.[10]

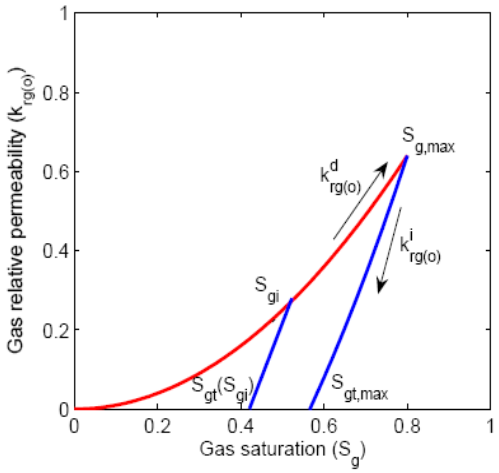

Figure 7: Parameters required in the evaluation of trapping and relative permeability hysteresis models.[10]

In Killough's method, the non wetting phase relative permeability along a scanning curve, such as the one depicted in Figure 7, is computed as:

$$K^{i}_{rg}(S_g) = \frac{K^{i}_{rg(o)} \times S_{g,norm} \times K^{d}_{rg(o)} \times S_{gi}}{K^{d}_{rg(o)} \times S_{g,\max}} \quad \text{..... (4)}$$

Where $K^{i}_{rg(o)}$ and $K^{d}_{rg(o)}$ represent the relative permeability values on the bounding imbibition and drainage curves, respectively.

S_{gi} is the initial gas saturation, $S_{g,max}$ is the maximum gas saturation from the bounding imbibition curve, and $S_{g,norm}$ is the normalized gas saturation computed as:

$$S_{g,norm} = S_g + \frac{(S_g - S_{gt,\max}) \times (S_{gt,\max} - S_g)}{S_{gi} - S_{gt,\max}} \quad \text{..... (5)}$$

Where $S_{gt,max}$ is the maximum trapped gas saturation, associated with the bounding imbibition curve.

2.5.3 Injection Pattern

The five-spot injection pattern seems to be the most popular onshore with a fairly close well spacing. Because many of the field applications are miscible operations, many wells will give a good control of the field pressure and thus of the WAG-injection performance. Inverted 9-spot patterns are also reported in DUWAG and the Hybrid WAG projects. [1]

2.5.4 Injection Gas Characteristics

The injection gases used in WAG projects today can be classified into roughly three groups: CO_2, hydrocarbons, and non-hydrocarbons (CO_2 excluded). CO_2 is an expensive gas and is generally used when miscible drive should be achieved, or if special options for deliverance exist. It is worth noticing that corrosion problems are often mentioned and seem impossible to avoid when using CO_2.[1]

Hydrocarbon gas is available directly from the production. For this reason all offshore WAG injections today use hydrocarbon gases, although the possibility of injecting CO_2 offshore is currently being investigated for environmental reasons.[1]

The type of injection gas also has been compared. CO_2 shows an average improved oil recovery of 10%, while hydrocarbon gas and nitrogen have an improved oil recovery of 8%. The higher recovery by CO_2 may be coupled to the fact that most CO_2 WAG injections are miscible, while the hydrocarbon gas WAG field tests in a large fraction are immiscible.[1]

2.5.5 Tapering

Tapering is increasing in the injection volume of water relative to at a later stage of the WAG injection to control channeling and breakthrough of gas.gas-to-water ratio during the flood progresses. This scheme is especially important when an expensive gas source is used. Tapering has generally been used, even in the very first WAG-injection field trials in the early 1960's [1], and has also proved effective in reducing CO_2 production and increasing the effectiveness of CO_2 injection. [5]

2.5.6 WAG Ratio

WAG refers to the ratio of a water to CO_2 in the process.The wetting state was found to be a major factor affecting flood performance, with the consequence that tertiary food in the water-wet laboratory model were dominated by gravity forces, while oil-wet tertiary floods were controlled by viscous fingering.[12]

Wettability effects have also been shown to affect the optimum WAG ratio.Water-wet bead packs show an optimum WAG ratio of 0:1 or continuous gas injection. Contrarily oil wet packs suggest an optimum WAG ratio of equal or 1:1 velocity ratios. Mixed-wet states indicate maximum recovery is a stronger function of slug size in secondary CO_2 recovery than in tertiary flooding. In addition, water-wet laboratory models indicate gravity forces dominate while in oil-wet tertiary floods, viscous fingering is a controlling factor.[3]

There are a number of different WAG schemes to optimize recovery. One of these processes called Hybrid-WAG where a large fraction of the pore volume of CO_2 to be injected is injected followed by the remaining fraction divided into 1:1 WAG ratios. Shell empirically evolved a similar process called the DUWAG (Denver Unit WAG) by comparing field results from the continuous injection and WAG processes.[3]

Injecting below equal velocity WAG ratio is viscously unstable while injecting above the equal WAG ratio creates stability at the expense of increasing trapped oil or displacement efficiency. Since the process can create water barriers or shielding effects, a WAG cycle can have a harmful effect on achieving maximum oil solvent contact time.[3]

2.5.7 Slug Size

Slug size refers to the cumulative of CO_2 injected during a CO_2 flood. The slug volume is usually expressed as a percentage of the hydrocarbon pore volume (%HCPV). Selecting an optimum CO_2 slug size is critical in a proper design of a hydrocarbon miscible flood.[13]

Generally, the more CO_2 injected, the greater the incremental oil recovery. However, a large CO_2 slug size diminishes the return of the project. The larger the CO_2 bank size, the greater the ultimate recovery, but the increment gets smaller and smaller. [5]

The optimum CO_2 slug size for a particular project will depend upon economic factors

such as crude price, CO_2 cost, and the amount and timing of the incremental recovery. The economic optimization process is carried out by systematically repeating simulation runs until optimum design parameters are achieved.[14]

The ultimate CO_2 slug size for any project does not have to be finalized at the start of the project. This decision can be made later in the life of the project when the operator has a better handle on crude price and production response. Also, it should be mentioned that the optimum solvent bank size should be determined on an individual pattern basis rather than on a total project evaluation.

2.5.8 Gravity Considerations in WAG

As suggested by Green and Willhite [15], the same density difference between injected gas and displaced oil that causes problems of poor sweep efficiencies and gravity override in these types of processes can be used as an advantage in dipping reservoirs. Gravity determines the 'gravity segregation' of the reservoir fluids and hence controls the vertical sweep efficiency of the displacement process.

Several North Sea WAG pilot results showed that gravity segregation can play a positive role with this process. Gas rising to the attic of a field displaces trapped oil and dense water settling into low structure areas can displace oil up to a producer.[6]

2.5.9 Laboratory requirements and Simulation

The ability to predict CO_2 performance through the use of reservoir simulation is a critical tool in designing and implementing a successful CO_2 injection project. Experience has shown that industry has developed simulation capability that can accurately predict CO_2 performance. To date industry has obtained sufficient production history under CO_2 flooding to calibrate and evaluate the effectiveness of reservoir simulators.[5]

Laboratory research and detailed reservoir simulation plays a very important role in the development and implementation of WAG injection projects.[6] The quality of the input data for reservoir simulations plays a key role in the quality of the predictions of WAG processes, including geological descriptions along with the reservoir rock and fluid properties. For compositional simulations phase behavior experiments in PVT cells, performed to develop a tuned equation of state model capable to match all

laboratory data, are required for a good characterization of the fluid components thermodynamic properties, and binary interaction coefficients.

Ideally, a full field, finely gridded, fully compositional coupled with surface facility calculations would be used to predict the performance of complex heterogeneous oil and gas condensate reservoirs.[6]

Studies of modeling WAG process indicate that in stratified dipping reservoirs with unfavorable layering, down-dip WAG can be more efficient than up dip gas injection, and that WAG is attractive in reservoirs with communicating layers, while SWAG (Simultaneous Water and Gas injection) is attractive in reservoirs with poor communicating layers.[6]

CHAPTER 3 SIMULATION PARAMETERS AND MODEL

In this chapter, the simulation parameters used in this thesis are presented. The process includes equations of state (EOS) model to describe the phase behavior of the reservoir fluid, PVT fluid properties and rock-saturation dependent properties such as relative permeability, rock properties, and the initialization of the simulation model to assess the volume of the original hydrocarbon in place.

3.1 Numerical Simulator

One of the concerns about the reservoir fluid model was to select the simulator that best represents CO_2 displacement process. Compositional simulators use EOS with theoretical parameters that are able to predict fluid behavior of hydrocarbon mixtures commonly encountered in oil and gas reservoirs.

The simulator used in this thesis was ECLIPSE 300 which is finite-difference compositional simulator with a cubic EOS. The ECLIPSE 300 compositional simulator is useful when an equation of state is required to describe reservoir fluid phase. This simulator reproduces the major mass-transport and phase-equilibrium phenomena associated with the miscible CO_2 flooding process. The ECLIPSE compositional simulator has several EOSs. These include the Redlich-Kwong, Soave-Redlich-Kwong, Soave-Redlich-Kwong 3-parameter, Peng-Robinson and Peng-Robinson 3-parameters.

3.2 Fluid Properties

The reservoir oil is undersaturated black oil with a stock tank gravity of 44.8 °API. Initial reservoir pressure and bubble point pressure are 6000 and 3224.65 psi respectively at a reference depth of 12,000 ft and 200°F. Table 1 summarizes basic reservoir and fluid data.

Table 1: Summary of reservoir data.

Reservoir Characteristics	Values
Formation	Tarbert and Ness
Average Depth	12000 ft
Initial reservoir pressure	6000 psia
Surface density	50 lb/ft^3
Oil Gravity	44.8 º API
Reservoir Temperature	200 º F
Oil viscosity at surface	0.695 cp
Bubble point pressure	3224.65 psia
Initial relative volume	2.0789 res BBL/STB
Relative volume at Bubble point pressure	2.2755 res BBL/STB
Minimum miscibility pressure	3224.65 psia

The Fluid characteristic is compositional PVT properties obtained from ECLIPSE package (2008) tutorial Nº 7.

Table 2 shows the fluid composition.

Initial reservoir pressure and bubble point pressure are 6000 and 3224.65 psi respectively at a reference depth of 12000 ft and 200 ºF.

The CO_2 minimum miscibility pressure was determined to be 3224.65 psia using the simple suggestion reported by Yellig and Metcalfe However [16], the authors suggest that if the bubble point of the oil is greater than the predicted MMP, then the MMP be set equal to the bubble point pressure, Figure 8.

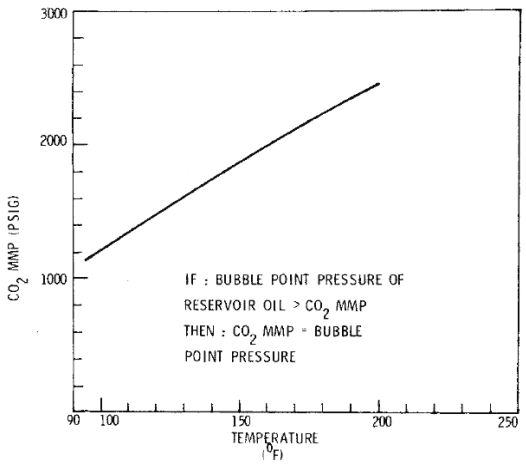

Figure 8: Temperature/bubble-point pressure of CO2 MMP correlation.[16]

Table 2: Reservoir fluid composition in mole fractions.

Component	Mol Fraction
CO_2	0.0500
C1	0.5000
C3	0.2000
C7	0.1500
C15	0.0799
C31	0.0199

3.3 Rock and Water properties

Rock and water properies are shown in table 3. the standard condition are 60 º F and 14.69 psia.

Table 3: Rock and water properties

Characteristics	**Values**
Rock Compressibility	$1*10^{-6}$ psi^{-1}
Water FVF at reference pressure	1.01 RB/STB
Water Compressibility	$3*10^{-6}$ psi^{-1}
Water viscosity at reference pressure	0.3 Cp

3.4 Equation-of-State Characterization

An essential part of a compositional reservoir simulation of a miscible EOR method is the prediction of the complex phase equilibrium during the processes. The objective of the fluid study was to tune an EOS that would reproduce the observed fluid behavior and production characteristics seen in field operations and to predict the CO_2 /oil phase behavior in the compositional simulation.

Cubic equations of state (EOS) have found widespread acceptance as tools which permit the convenient and flexible calculation of the phase behavior of reservoir fluids. They facilitate calculations of the complex behavior associated with rich condensates, volatile oils and gas injection processes.[17]

In this thesis a tuned EOS model with 5 components from ECLIPSE (2008) tutorial N^{o} 7 was used. This tuned model helps in accurate characterization of reservoir fluid. The Peng Robinson EOS was chosen to generate the EOS model and the Lohrenz-Bray-Clark (LBC) model as viscosity model.

3.5 Relative Permeability

The complete SCAL data for my work were taken from ECLIPSE (2008) tutorial N^{o} 7. The two-phase oil relative permeability data (oil saturation function) are shown in Figure 9. I used the default model in ECLIPSE as three phase interpolation model to compute oil relative permeabilities in three-phase system.

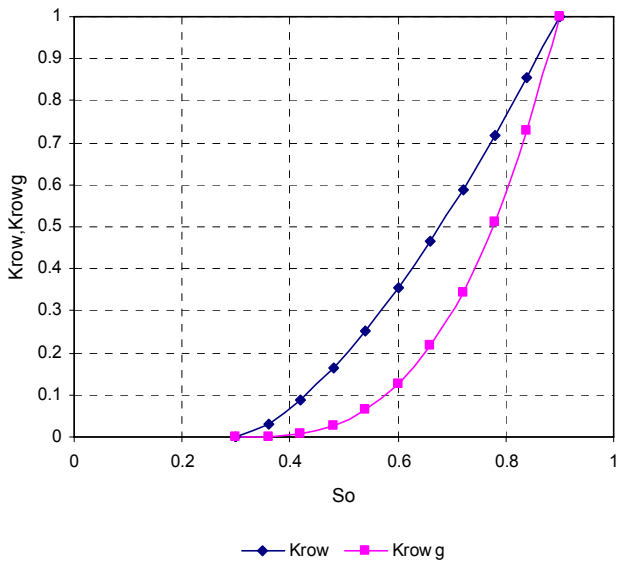

Figure 9: Relative permeability for an oil-water (K_{row}) and oil-gas-connate water (K_{rowg}) system.

For simplicity, I follow the assumption that water relative permeability is a function of water saturation alone, and independent of the saturation history. The water relative permeability data (Water Saturation function) from ECLIPSE (2008) tutorial N^{o} 7 are shown in Figure 10.

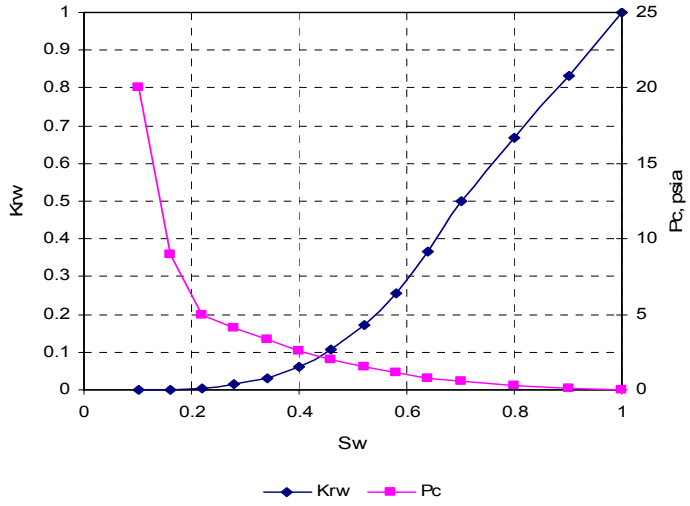

Figure 10: Water relative permeability data.

I have assumed that the gas saturation function (Figure 11) is calculated using Killough hysteresis model since I don't have imbibition and drainage bounding relative permeability curves.

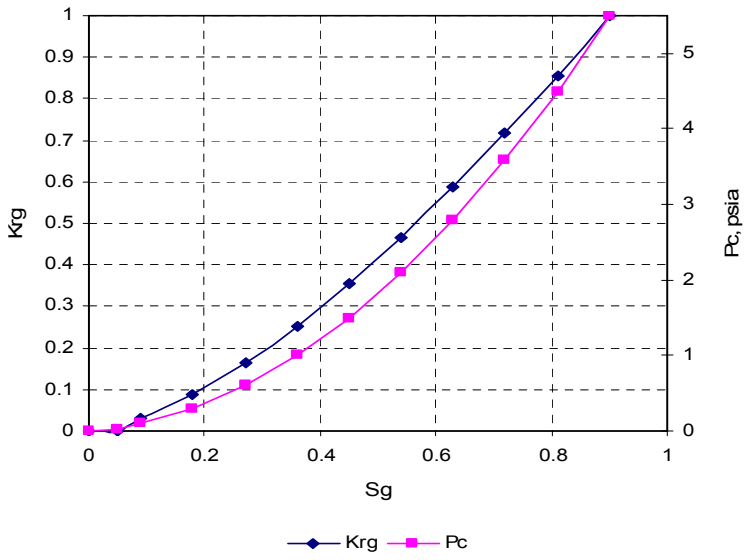

Figure 11: Gas relative permeability data.

3.6 Reservoir Simulation Model

The reservoir model for this study is an upscaled version of the SPE 10 comparative solution project model. (See Appendix A for model description and Appendix B for Work Flow of the Model Preparation). At the fine geological model scale, the model is described on a regular Cartesian grid.

The model dimensions are 1,200 X 2,200 X170 ft. The top 70 ft (35 layers) represent the Tarbert formation and the bottom 100 ft 50 layers) represent Upper Ness. The fine-scale cell size is 20 X 10 X 2 ft. The model has 60 X 220 X 85 cells ($1.122X10^6$ cells).

The upscaled cell size is 40 X 20 X 2 ft. The upscaled model has 30 X 110 X 85 cells (280,500 cells). There are 279767 active cells. The 40 x 20 grid design provided acceptable results when compared with the fine-scale model. See appendix C for upscaling. Figure 12 presents the well locations and the porosity distribution for the whole model.

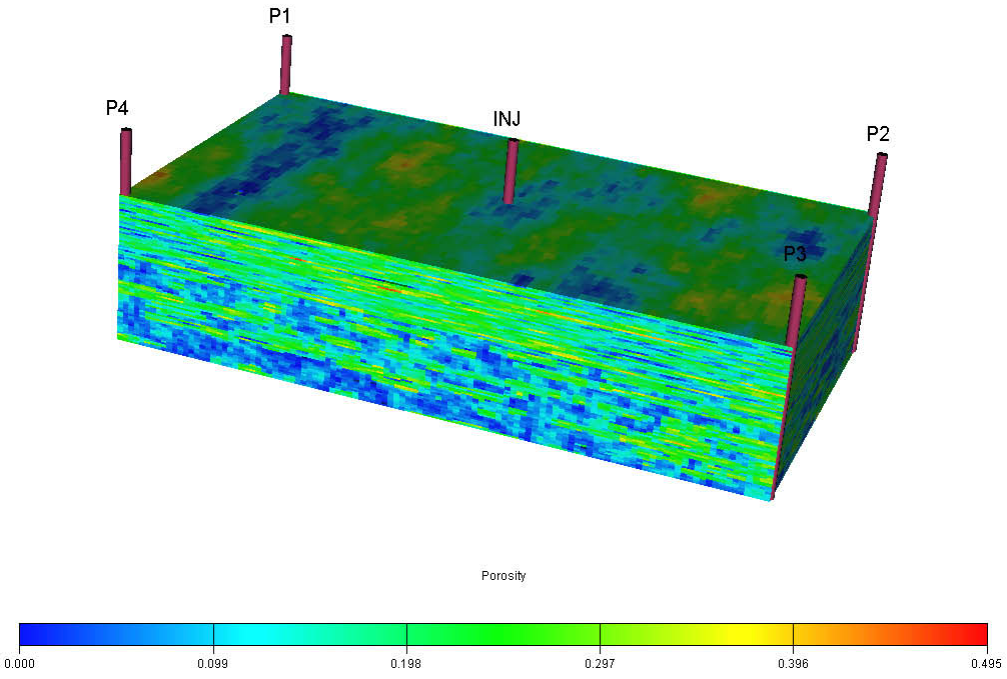

Figure 12: Porosity for the whole model.

Well pattern is five spots. There are four production wells and one central injector. All wells are vertical and completed in all the layers of the simulation model. The well locations are shown in Table 4.

Table 4: Well Locations.

Well Name	X location, ft	Y location, ft
Injection Well I1	600	1100
Production Well P1	0	0
Production Well P2	1200	0
Production Well P3	1200	2200
Production Well P4	0	2200

3.7 Initial Conditions

The equilibration method was chosen for model initialization. This is the simplest and most commonly used method for initializing a model. The reservoir model was initiated at a uniform pressure of 6000 psia and constant temperature of 200 ºF at datum depth of 12000 ft. The WOC assumed to be 13000 ft. The model provided an estimate of OOIP of 12.27 million BBLS at initialization.

CHAPTER 4 EFFECT OF WAG PARAMETERS

In this chapter, the optimization of WAG processes is discussed. The effect of WAG ratios, CO_2 slug sizes and CO_2 injection rate on the ultimate recovery are analyzed to make conclusions and recommendations.

4.1 Studying the effect of WAG Ratio and CO_2 slug size

Two of the most important design issues for WAG process are the WAG ratio and the amount of gas injection or slug size. Various compositional simulations were conducted to study the effect of these important parameters.

A series of WAG ratio and slug sizes sensitivities were compared. Water alternating with CO_2 injections at four different WAG ratios (2:1, 1.25:1, 1:1, and 0.5:1) was performed. The runs evaluated CO_2 slug sizes at 5, 10, 12.5, and 15% HCPV. The total number of runs was 16 runs and the average simulation time was 36 hours per run. Water and CO_2 were injected at rate of 5000 BBL/D and 3000 Mscf /D, respectively. The producers are constrained by bottom-hole pressure and operated with a minimum constraint value of 40000 psi.

The gas and water injections were carried out in two cycles (two HCPV increments of CO_2 slug), injecting both fluids in the same well. After injection of each CO_2 increment, injection was switched to water until its increment volume was complete. Alternate injection of the two fluids was continued until the total desired CO_2 slug volume had been injected. WAG calculations are enclosed in appendix D.

Model results showed sensitivity to the WAG ratio and slug sizes used. Figure 13 throght 16 show comparison of the cumulative oil recovery from the entire model for constant WAG ratios after injection of 5, 10, 12.5, and 15% HCPV of CO_2.

Each figure presents the cumulative oil recovery as a function of slug size at constant WAG ratio. These figures show the dependence of cumulative oil production on the volume of the injected CO_2 slug. The larger the CO_2 slug size, the greater the

cumulative oil recovery. After a certain slug size (optimum slug size of 12.5%), however, increment gets smaller and smaller and in some case even decreases.

Figure 17 through 20 show comparison of the cumulative oil production from the entire model for different WAG ratios after injection of 5, 10, 12.5, and 15% HCPV of CO_2. Each figure presents the cumulative oil recovery as a function of WAG ratio at constant slug size. The highest cumulative recovery is obtained at a WAG ratio flood of 2:1 for all cases.
The effect of slug size on the cumulative oil recovery is summarized in figure 21. The optimum slug size can be determined by examining this figure.

Figure 22 through 24 show oil production rates from the entire model for 10, 12.5, and 15% HCPV of CO_2. Cumulative oil recoveries as line plots for these three slugs are compared, figure 25 through 27. Figure 28 & 29 compare cumulative oil and oil rate between continuous CO_2 injection and WAG for the entire model. The effectiveness of the WAC can be seen from these figures.

Figures 30 through 34 show 2D view of the oil saturation distribution after injecting 5, 10, 12.5, and 15% HCPV of CO_2 for WAG ratio of 2:1, 1.25:1, 1:1, and 0.5:1.
These figures indicate that the final oil distribution and the shape of the swept portion of the reservoir after the WAG posses is a strong function of WAG ratio and slug sizes in addition to the reservoir heterogeneity.

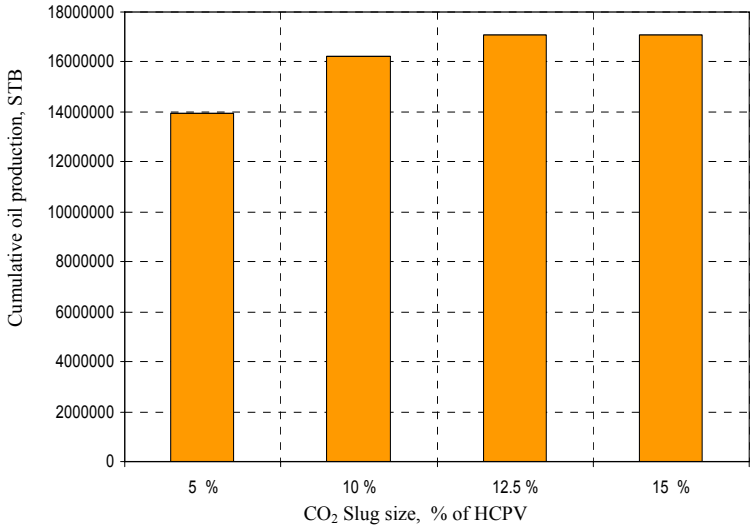

Figure 13: Cumulative oil production for different slug sizes at 2:1 WAG ratio.

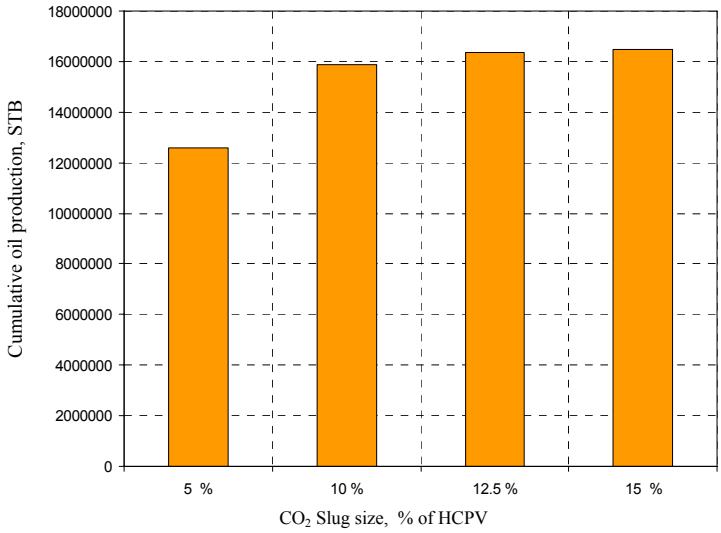

Figure 14: Cumulative oil production for different slug sizes at 1.25:1 WAG ratio.

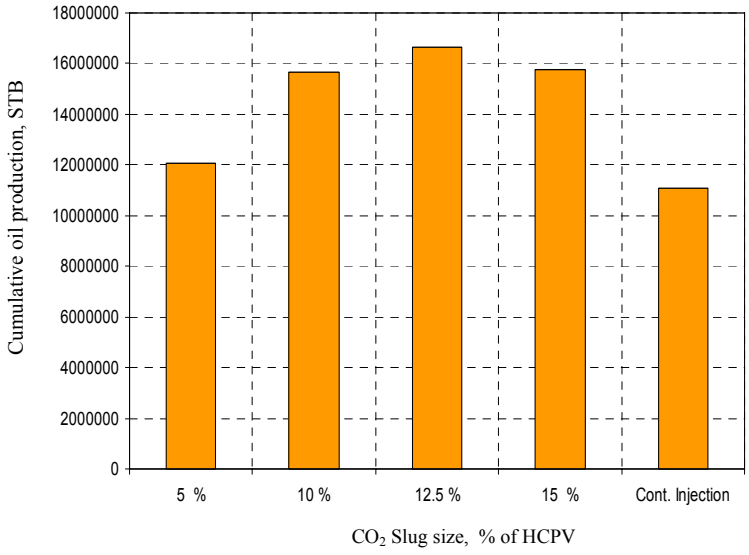

Figure 15: Cumulative oil production for different slug sizes at 1:1 WAG ratio.

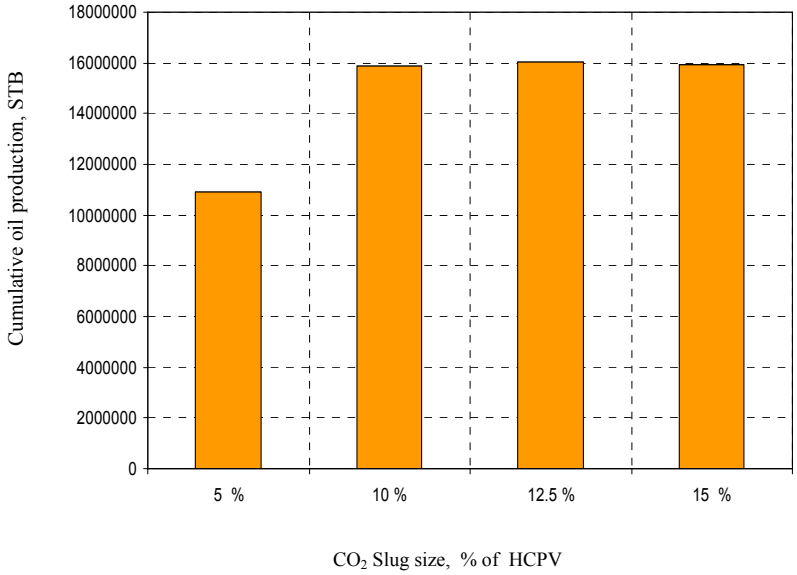

Figure 16: Cumulative oil production for different slug sizes at 0.5:1 WAG ratio.

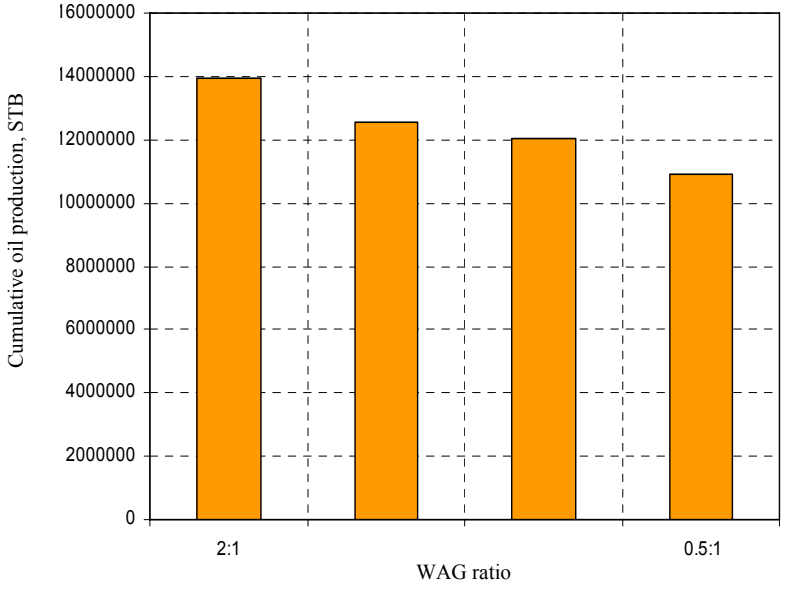

Figure 17: Cumulative oil production for different WAG ratios after injection of 5% HCPV of CO2.

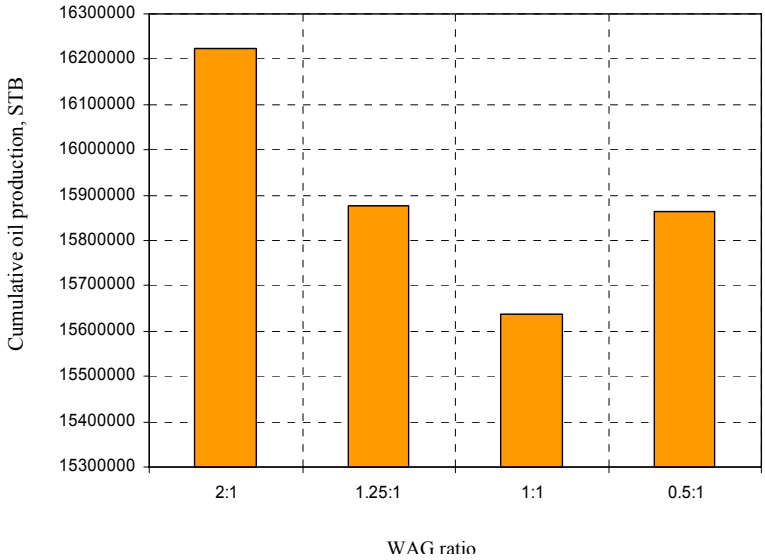

Figure 18: Cumulative oil production for different WAG ratios after injection of 10% HCPV of CO_2.

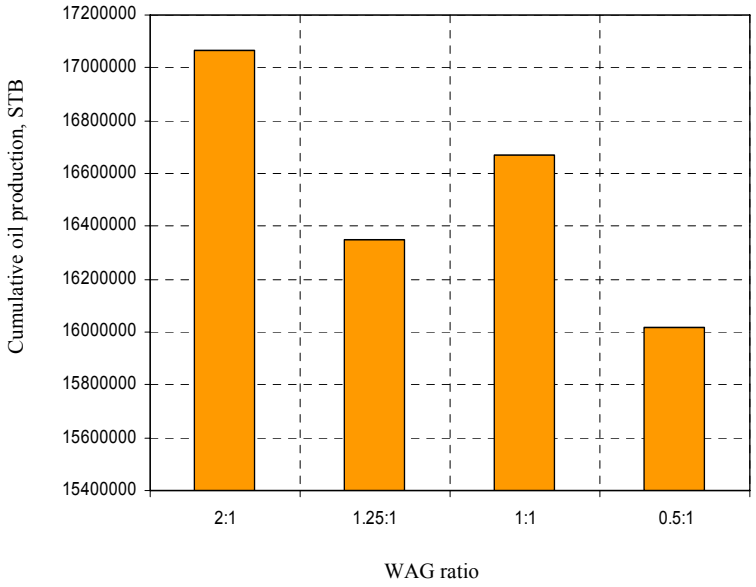

Figure 19: Cumulative oil production for different WAG ratios after injection of 12.5% HCPV of CO_2.

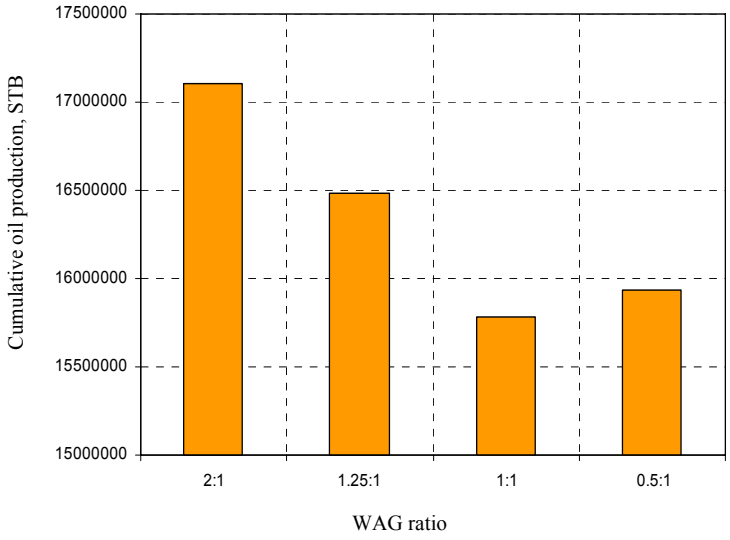

Figure 20: Cumulative oil production for different WAG ratios after injection of 15% HCPV of CO_2.

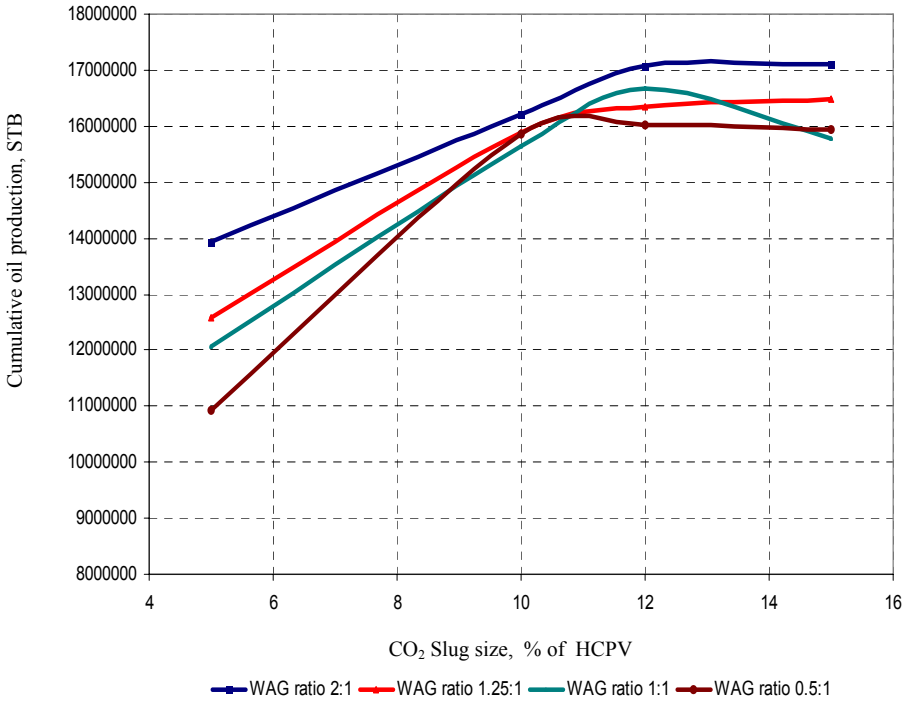

Figure 21: Effect of slug size on cumulative oil recovery.

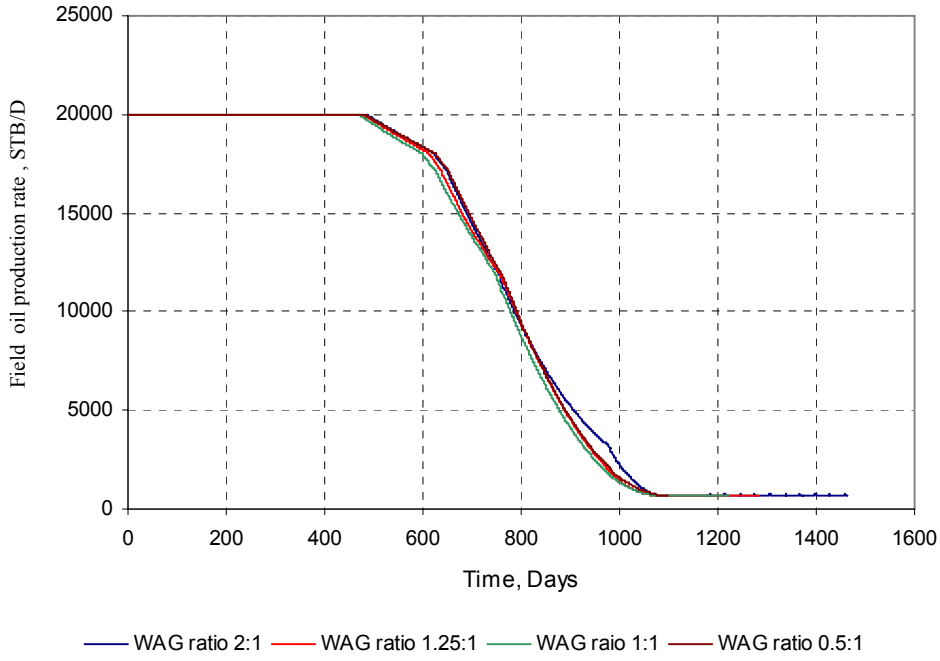

Figure 22: Field oil production rate for 10% CO_2 total slug size.

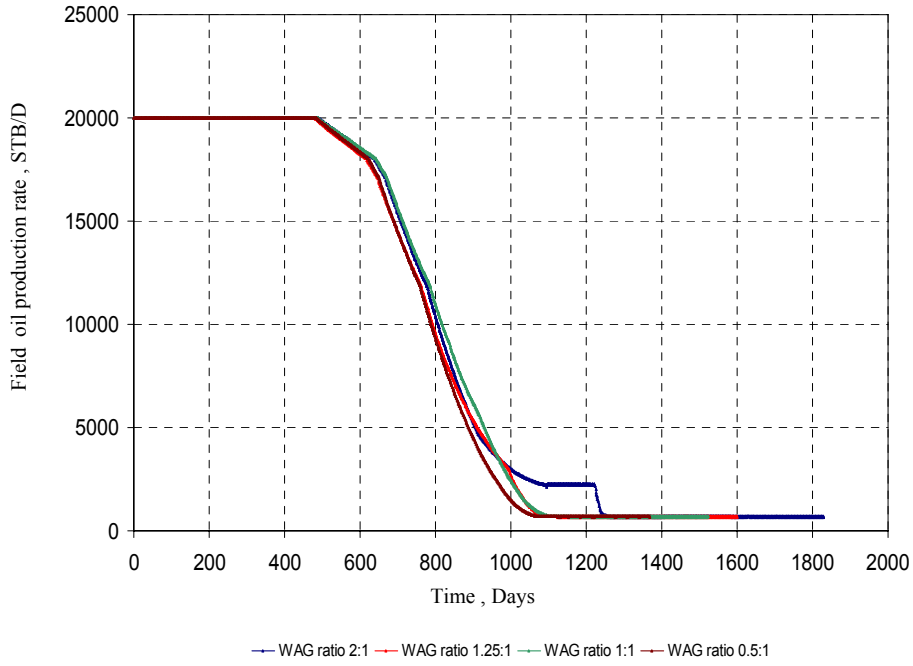

Figure 23: Field oil production rates for 12.5% CO_2 total slug size.

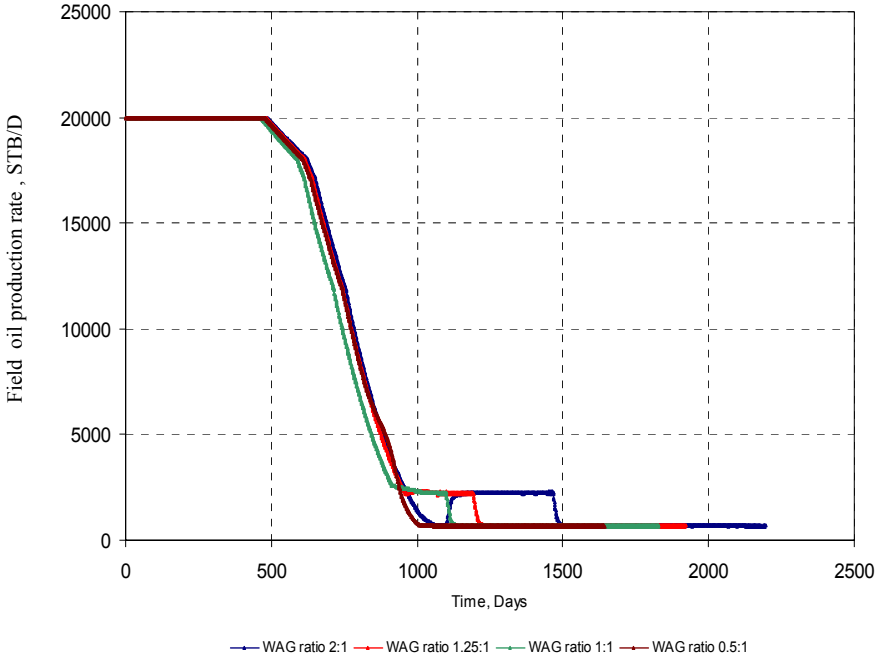

Figure 24: Field oil production rates for 15% CO_2 total slug size.

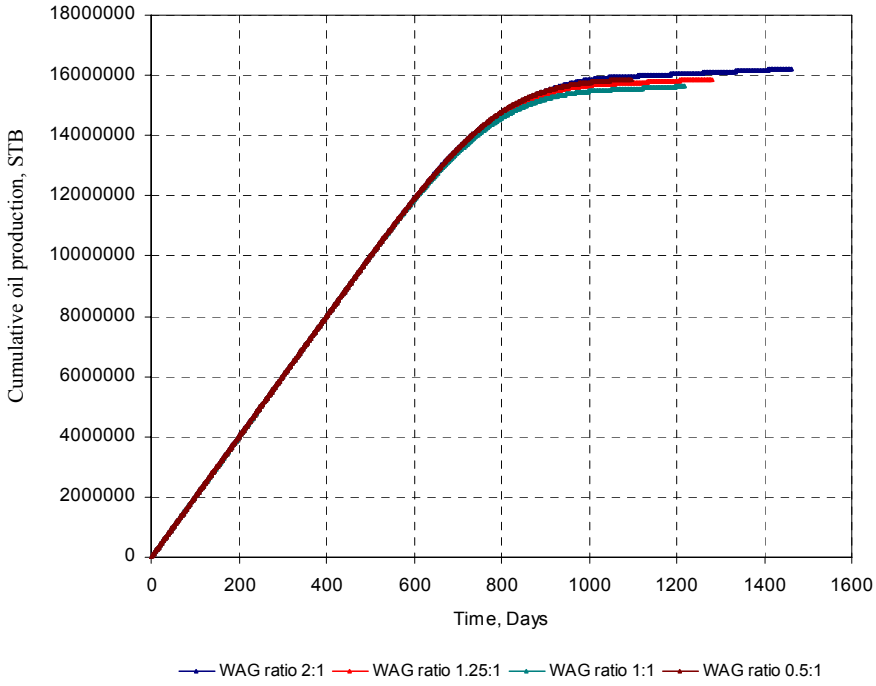

Figure 25: Field cumulative oil production for 10% CO_2 total slug size.

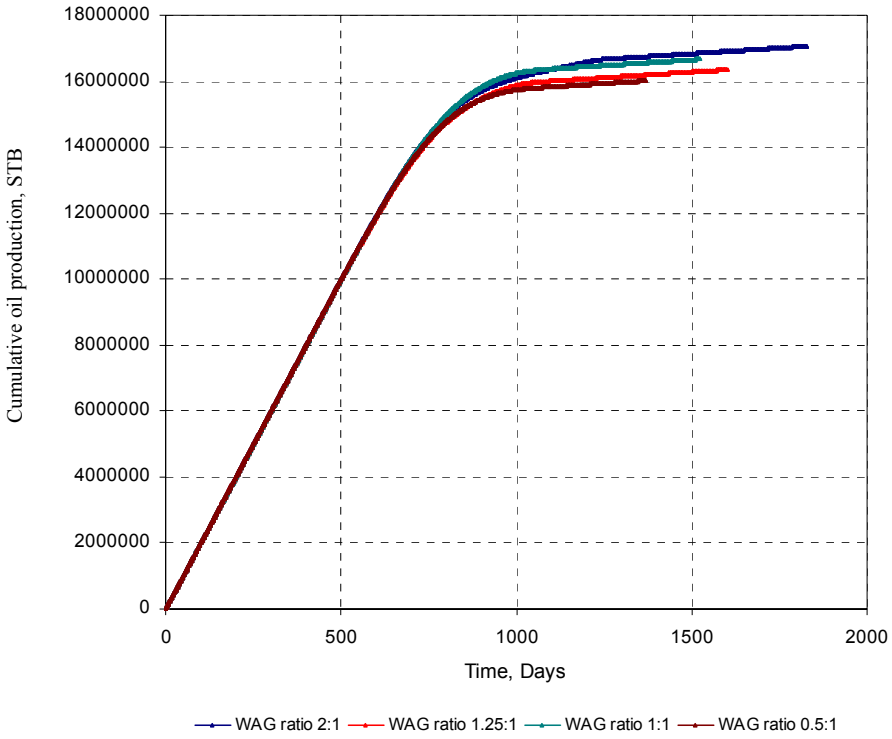

Figure 26: Field cumulative oil production for 12.5% CO_2 total slug size.

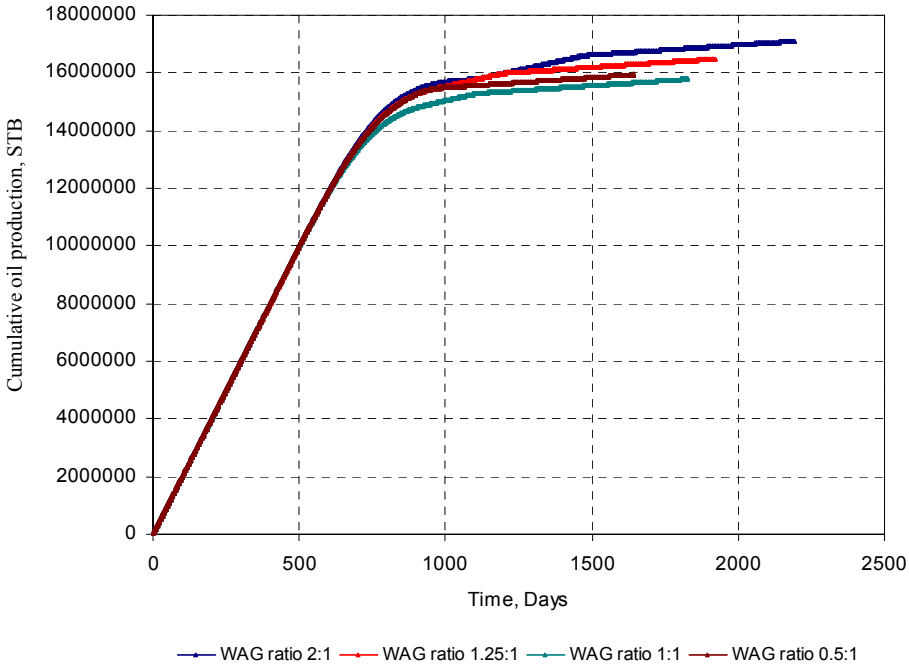

Figure 27: Field cumulative oil production for 15% CO_2 total slug size.

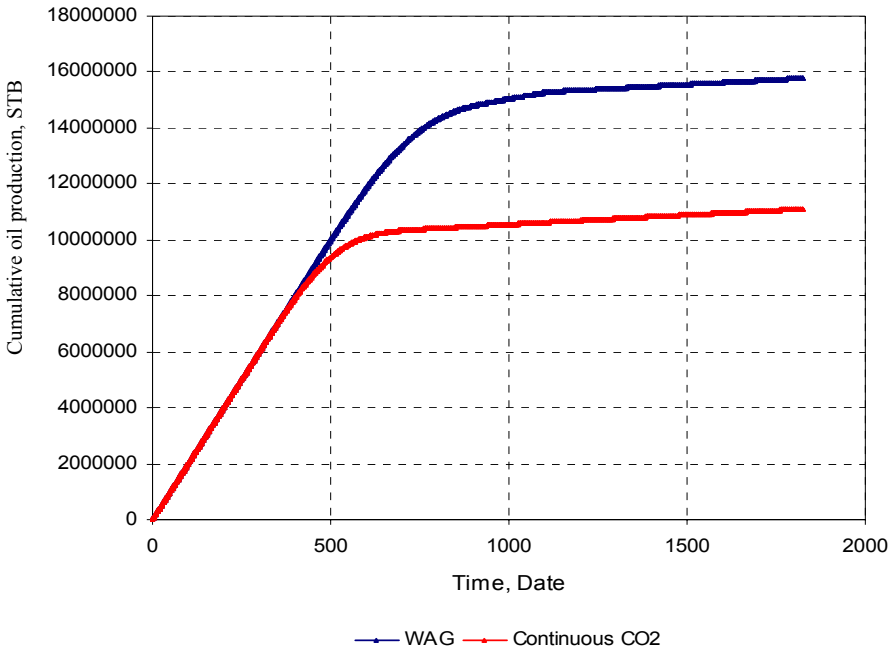

Figure 28: Cumulative production from WAG as compared with continuous CO_2 injection for 15 % slug size snd 1:1 WAG ratio.

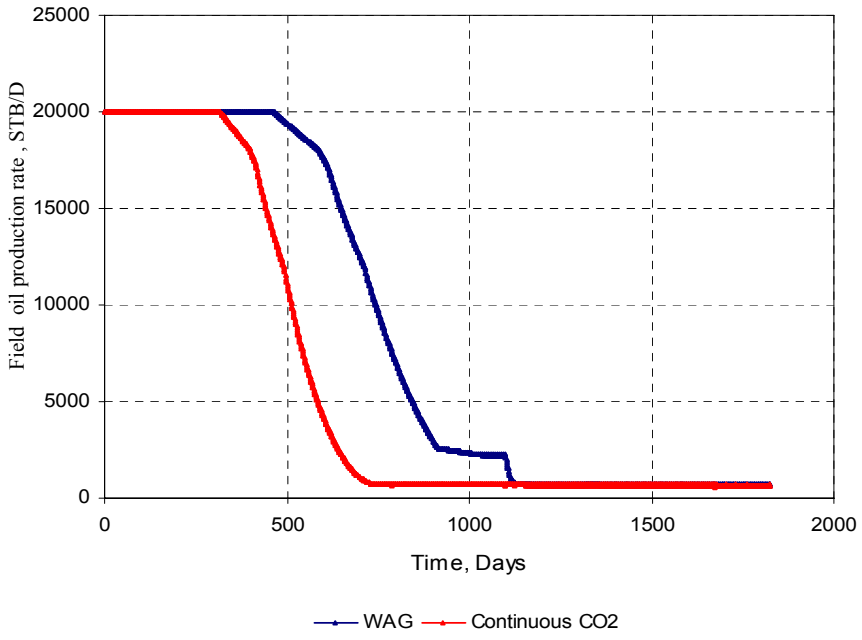

Figure 29: Oil production rate from WAG as compared with continuous CO_2 injection for 15 % slug size snd 1:1 WAG ratio.

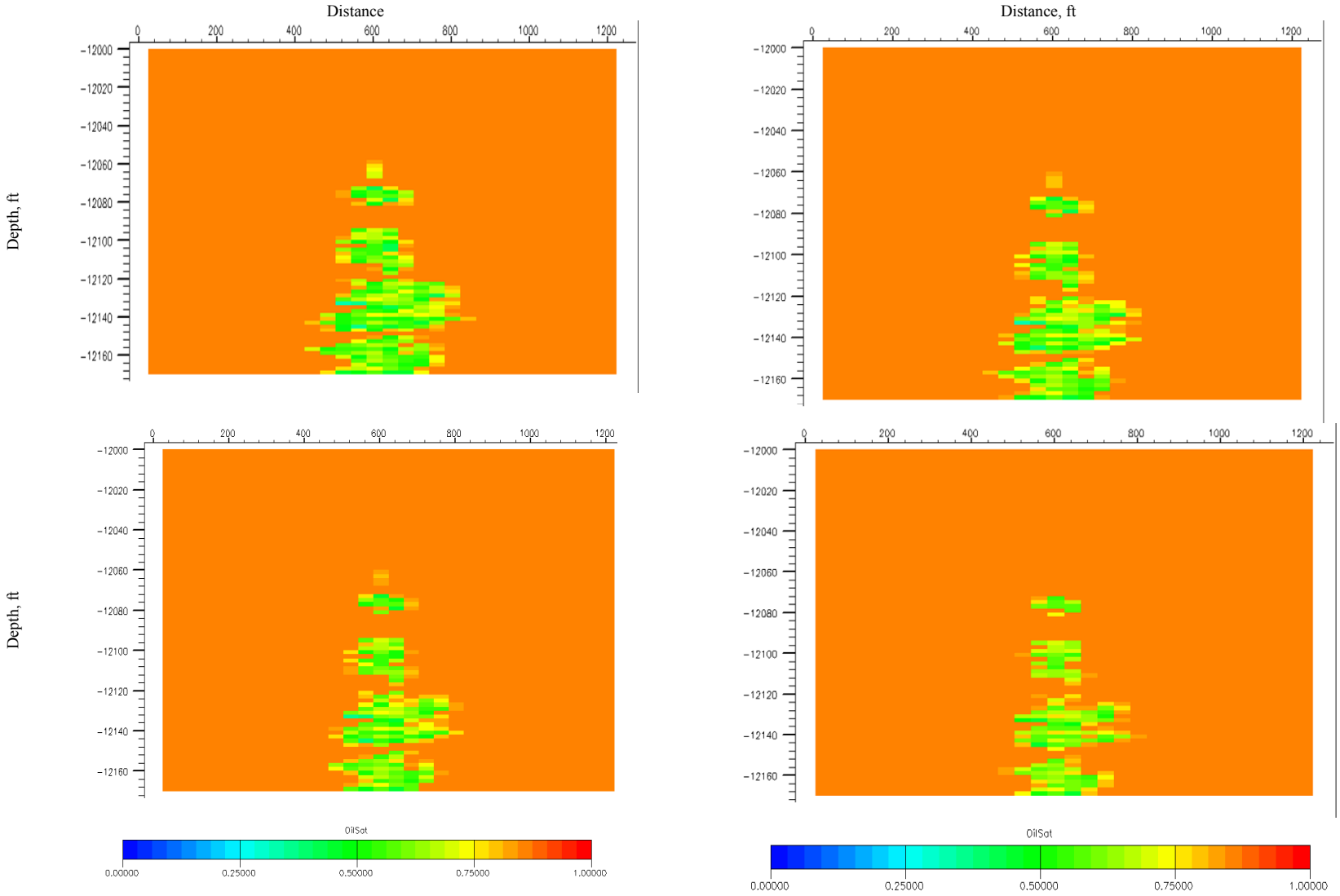

Figure 30: 2D view of the oil saturation distribution after injecting 5 % HCPV slug size of CO_2 with WAG ratios of (2:1 Upper left, 1.25:1 Upper right, 1:1 lower left, 0.5:1 Lower right), cross section at the injector.

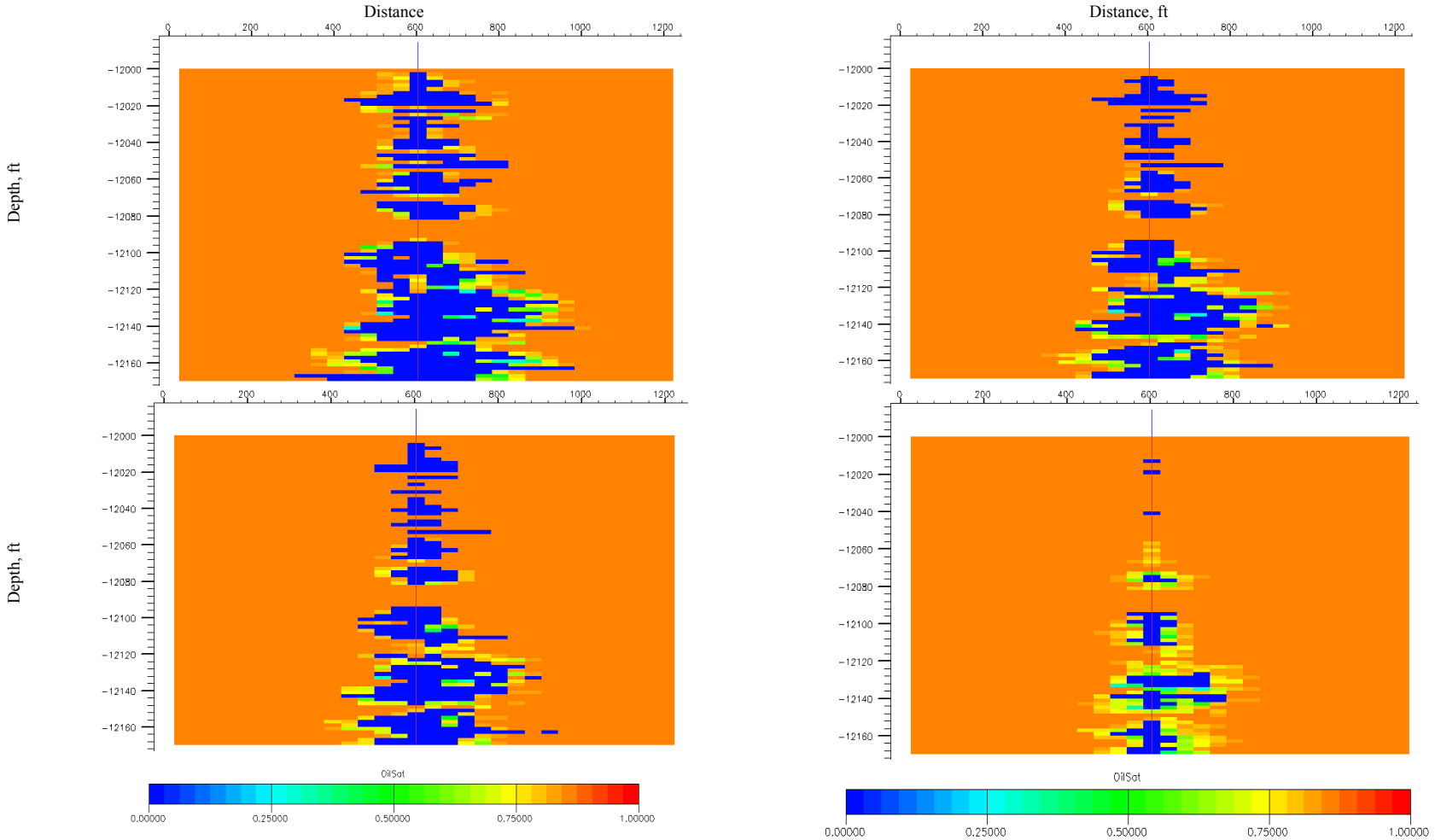

Figure 31: 2D view of the oil saturation distribution after injecting 10 % HCPV slug size of CO_2 with WAG ratios of (2:1 Upper left, 1.25:1 Upper right, 1:1 lower left, 0.5:1 Lower right), cross section at the injector.

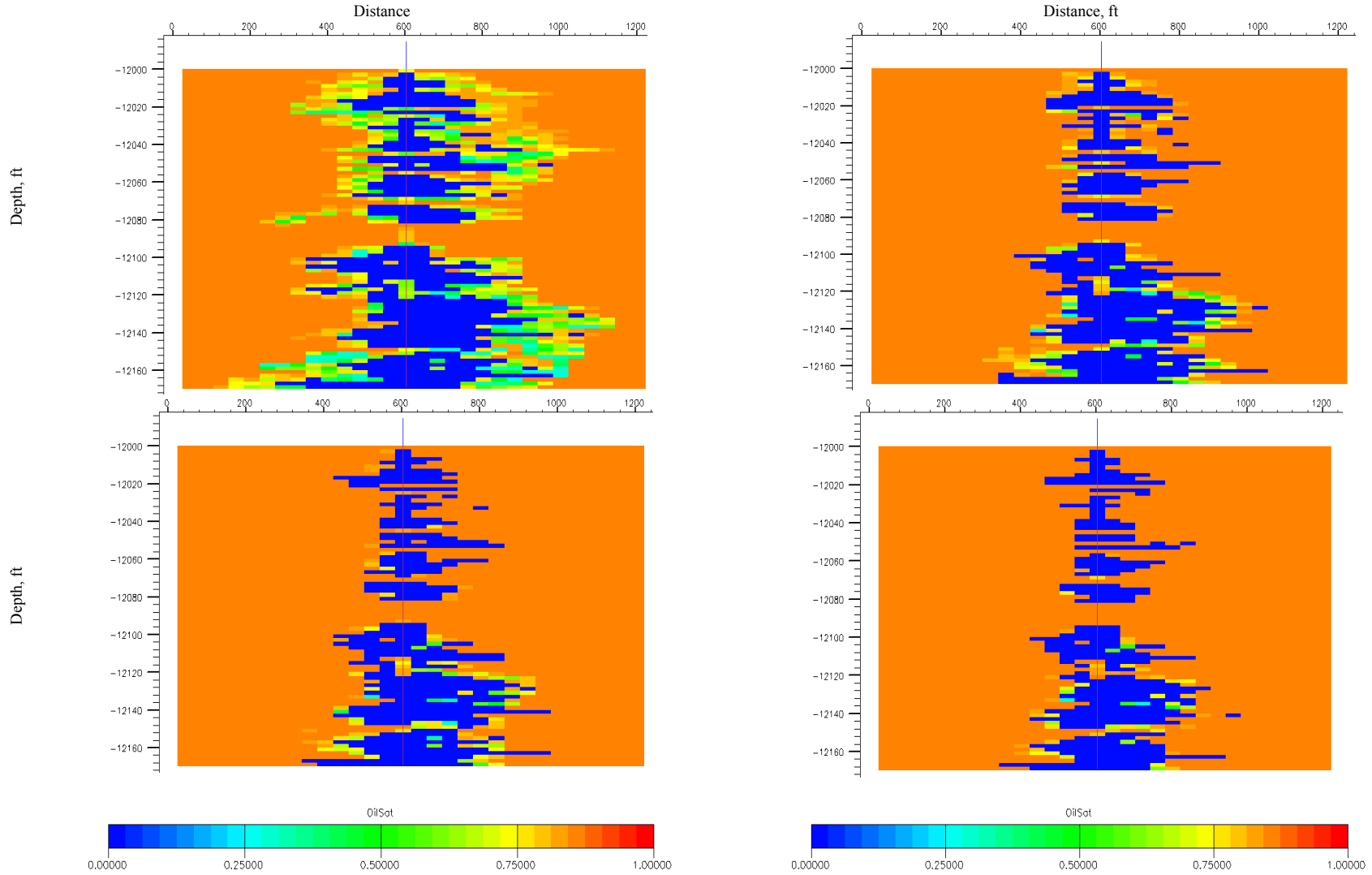

Figure 32: 2D view of the oil saturation distribution after injecting 12.5 % HCPV slug size of CO_2 with WAG ratios of (2:1 Upper left, 1.25:1 Upper right, 1:1 lower left, 0.5:1 Lower right),cross section at the injector.

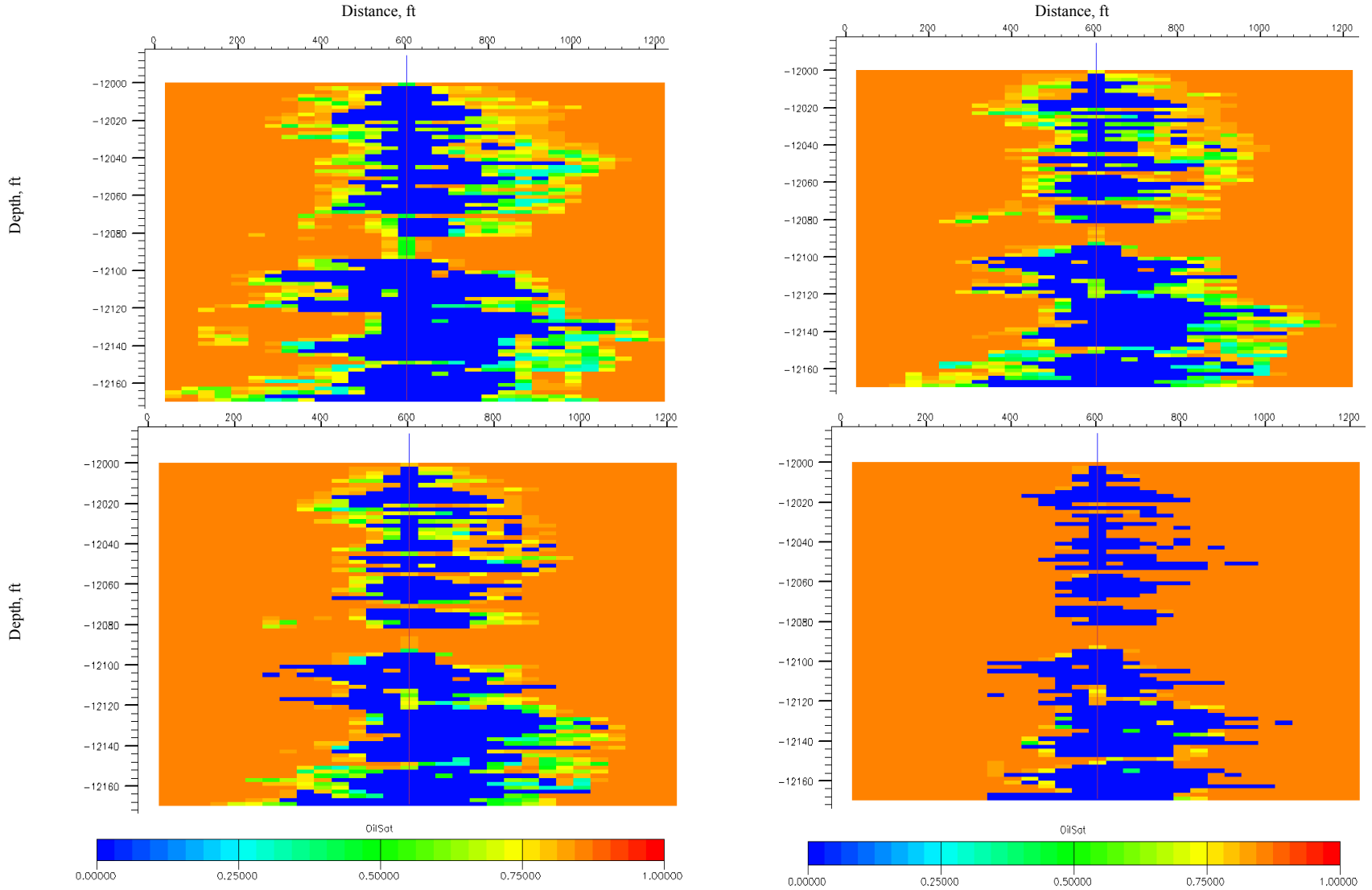

Figure 33: 2D view of the oil saturation distribution after injecting 15 % HCPV
slug size of CO_2 with WAG ratios of (2:1 Upper left, 1.25:1 Upper right, 1:1 lower left, 0.5:1 Lower right), cross section at the injector.

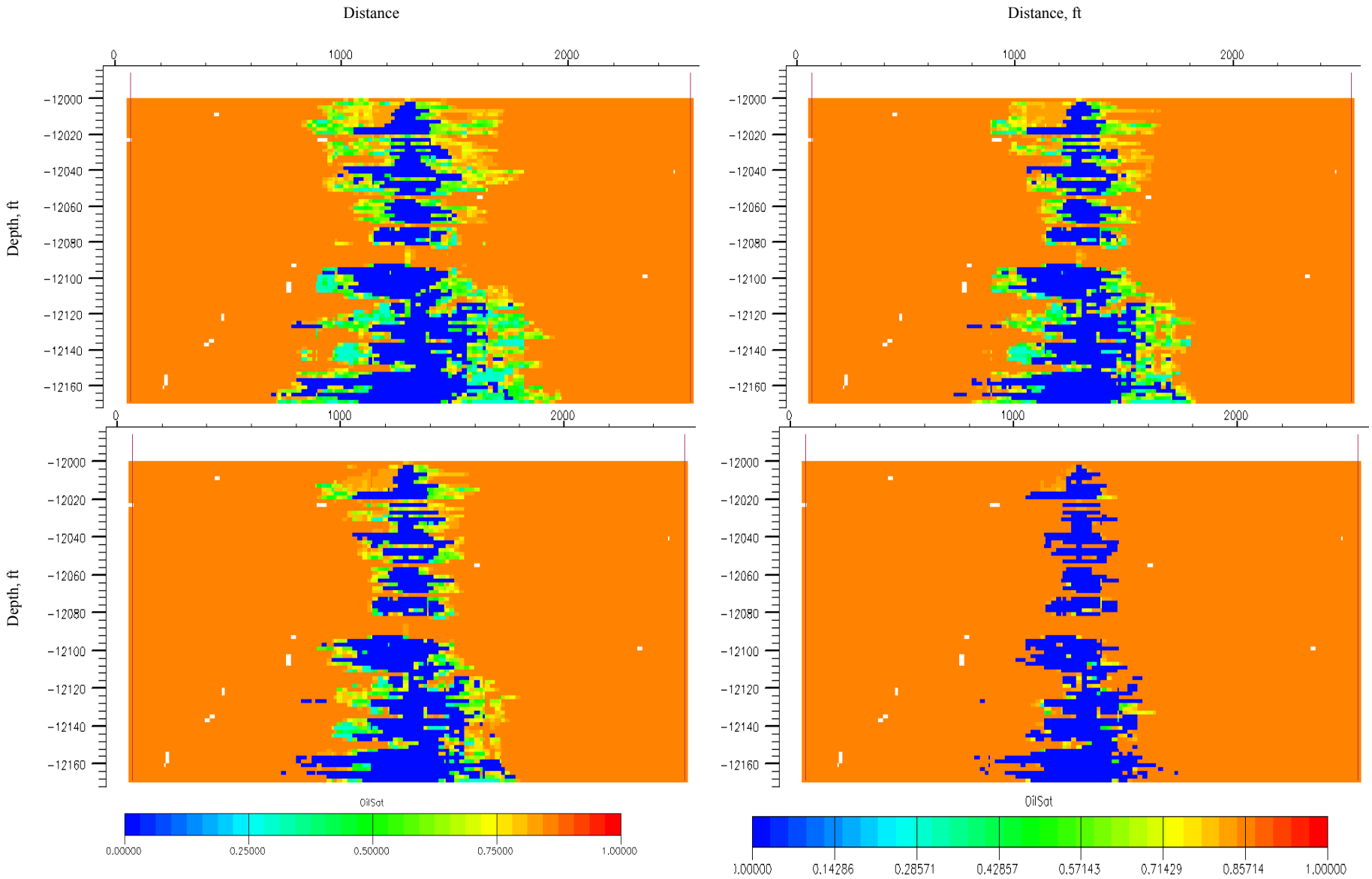

Figure 34: 2D view of the oil saturation distribution after injecting 15 % HCPV.
slug size of CO_2 with WAG ratios of (2:1 Upper left, 1.25:1 Upper right, 1:1 lower left, 0.5:1 Lower right), cross section at P2-Injector-P4.

4.2 Studying the effect of CO_2 Injection Rate

To investigate the effect of the injection rate on the WAG process, four sensitivities were performed at a WAG ratio of 1:1 using constant rates of 2000, 3000, 4000 and 5000 Mscf/D respectively of CO_2 and 5000 BBL/D of water. The runs evaluated CO_2 slug sizes at 12.5 % HCPV.

As the previous runs, WAG processes used two HCPV increments of CO_2 slug. After injection of each CO_2 increment, injection was switched to water until its increment volume was complete. Alternate injection of the two fluids was continued until the total desired 12.5 % HCPV of CO_2 slug volume had been injected. Figure 35 indicates that the recovery from WAG changes as a function of the injection rate. Cumulative oil production decrease as injection rate increases which is most likely a result of viscous fingering. Comparison between cumulative oil recovery obtained from these runs is shown in figure 36.

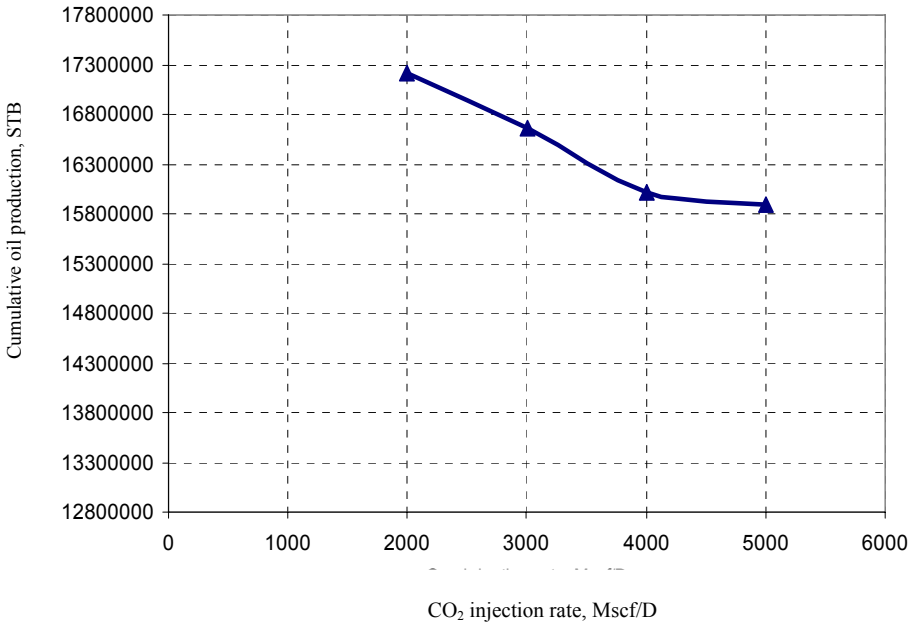

Figure 35: Oil recovery at WAG ratio of 1:1 and 12 % slug size as a function of injection rates.

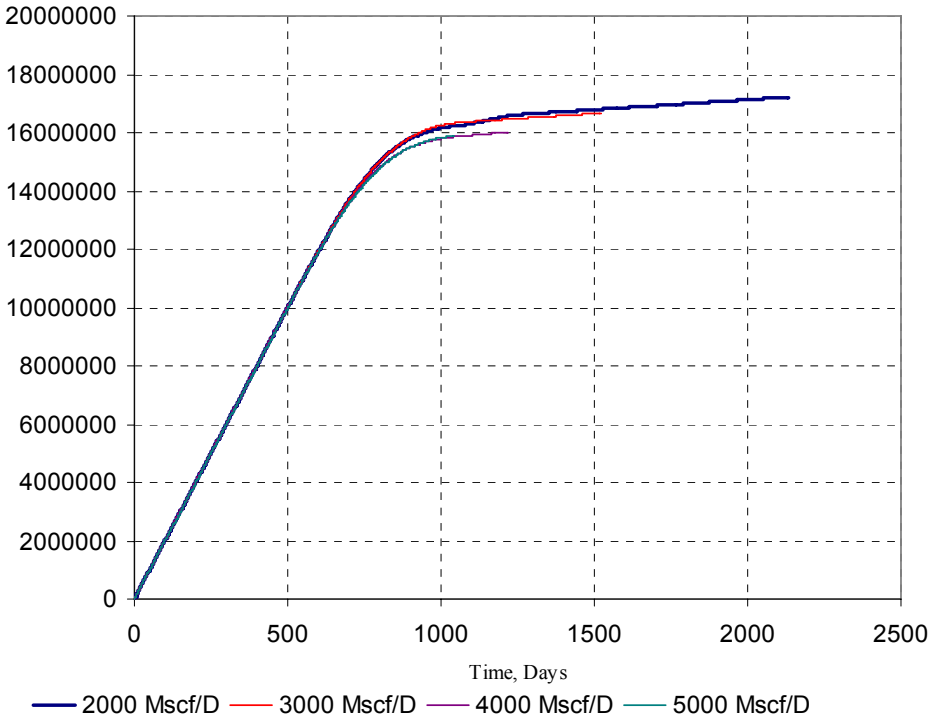

Figure 36: Cumulative oil production as a function of CO_2 injection rate.

CHAPTER 5 CONCLUSIONS AND RECOMMENDATIONS

5.1 Summary and Conclusion

Results from the sensitivity runs led to the following conclusions:

1) Recovery from a WAG process is a function of the injection rate as well as WAG ratio and the CO_2 slug.

2) The larger the CO_2 slug size, the greater the cumulative oil recovery, but at certain value (optimum slug size) increment gets smaller and smaller and in some cases even decreases.

3) At the same slug size and WAG ratio, increasing injection rate decreases total oil recovery in such stratified reservoir.

4) For this model, sensitivity results showed that the highest cumulative oil recovery is obtained at a WAG ratio of 2:1.

5) The final oil distribution and the shape of the swept portion of the reservoir after the WAG posses is a strong function in the above parameters in addition to the reservoir heterogeneity. So, it is important to have a good understanding of reservoir heterogeneities in designing a successful WAG process.

6) The WAG parameters influence in different ways the recovery efficiency from the high and low permeability layers. The higher permeability layers responded first to the process.

7) The cumulative oil recovery obtained with the continuous CO_2 flood was low compared to the WAG scheme.

8) Conducting numerous sensitivity analyses through the use of reservoir simulation is very important to predict and optimize the WAG process.

5.2 Recommendations

1) Since the optimum CO_2 slug size for a particular project will depend upon economic factors such as crude price, CO_2 cost, and the amount and timing of the incremental recovery, economic sensitivities must be performed to determine the optimum CO_2 slug size.

2) Alternative processes, like Hybrid-WAG and DUWAG should be tried during optimization of WAG.

3) The detailed laboratory studies should be coupled with reservoir simulation to insure successful WAG design.

ABBREVIATIONS AND NOMENCLATURE

Abbreviations

API	= American Petroleum Institute
BBL/D	= Barrel per Day
BHP	= Bottom Hole Pressure
CO_2	= Carbon dioxide
DUWAG	= Denver Unit WAG
EOR	= Enhanced Oil Recovery
EOS	= Equation of state
ESP	= Electrical Submersible Pump
HC	= hydrocarbon
HCPV	= Hydrocarbon Pore Volume
IOR	= Improved Oil Recovery
KH	= Average permeability * layer thickness
MMP	= Minimum Miscibility Pressure
Mscf /D	= Thousands standard cubic feet per Day
OOIP	= Oil Originally In Place
PV	= Pore Volume
PVT	= Pressure Volume Temperature
SCAL	= Special Core Analysis
SCF/STB	= Standard Cubic Feet Stock Tank Barrel
SPE	= Society of Petroleum Engineers
SWAG	= Simultaneous Water and Gas injection
WAG	= Water Alternating Gas

Nomenclature

μ_g	= Gas viscosity
μ_o	= Oil viscosity
Bg	= Gas formation volume factor

E_h = Horizontal sweep efficiency

E_m = Microscopic displacement efficiency

E_v = Vertical sweep efficiency

$K_{drg(o)}$ = Relative permeability values on the bounding drainage curves

$K^d_{ro(g)}$ = Oil relative permeability for a system with oil, gas at connate water

$K_{irg(o)}$ = Relative permeability values on the bounding imbibition curve

$K^i_{ro(w)}$ = Imbibition oil relative permeability for a system with oil and water

K_{rg} = Gas relative permeability

K_{ro} = Oil relative permeability

Kv/K_h = Horizontal to vertical permeability

K_x = Permeability in X direction

K_y = Permeability in Y direction

K_z = Permeability in Z direction

M = Mobility ratio

P_c = Capillary pressure

P_r = Reduced Pressure

R_f = Oil recovery

Sg = Gas saturation

$S_{g,max}$ = Maximum gas saturation from the bounding imbibition curve

$S_{g,norm}$ = Normalized gas saturation computed

S_{gi} = Initial gas saturation

$S_{gt,max}$ = Maximum trapped gas saturation, associated with the bounding imbibition curve.

S_{hy} = Maximum non-wetting phase saturation reached in the run

S_{ncrd} = Critical saturation of the drainage curve

S_{ncri} = Critical saturation of the imbibition curve

S_{ncrt} = Trapped critical saturation

S_{nmax} = Maximum saturation

S_o = Oil saturation

T_r = Reduced Temperature

Z = Compressibility factor

REFERENCES

[1] Christensen, J R, Stenby, E H, Skauge, A, “Review of the WAG field experience”, SPE 71203, revised paper 39883, presented at the 1998 SPE International petroleum conference and exhibition of Mexico, Villhermosa, March 3-5, 1998.

[2] William C .Lyons, PH.D., P .E.”Standard Handbook of Petroleum and Natural Gas Engineering” Volume 6, 1996.

[3] Rogers, J D, Grigg, R B, “A literature analysis of the WAG injectivity abnormalities in the CO_2 process”, SPE 59329, presented at the 2000 review SPE/DOE Improved Oil Recovery symposium on held in Tulsa, OK, April 3-5, 2000.

[4] Surguchev, L. M., Korbρl, R., Haugen, S., Krakstad, O.S.: "Screening of WAG Injection Strategies for Heterogeneous Reservoirs," paper SPE 25075 presented at the 1992 SPE European Petroleum Conference, Cannes, France, Nov. 16-18.

[5] Hadlow, R E, “Update of Industry experience with CO_2 Injection”, SPE 24928, presented at 1992 SPE annual technical conference and exhibition, Washington D C, Oct 4-7,1992.

[6] Sanchez, N L, “Management of Water Alternating Gas (WAG) Injection Projects”, presented at the 1999 SPE Latin American and Caribbean Petroleum Engineering Conference held in Caracas, Venezuela, 21-23 April 1999.

[7] Tanner, C S, Baxley, P T, Crump III, J C, Miller, W C, “Production performance of the Wasson Denver Unit CO_2 flood”, SPE/DOE 24156, presented at the SPE/DOE eighth symposium on Enhanced Oil Recovery held in Tulsa, OK, Aug 22-23, 1992.

[8] Helm, L. W.:” Status of $C0_2$ and Hydrocarbon Miscible Oil Recovery Methods,” paper SPE 5560.

[9] Gorell, S B, “Implications of water alternate gas injection profile control and injectivity”, SPE 20210, presented at the 1990 SPE/DOE symposium on Enhanced Oil Recovery held in Tulsa, OK, April 22-25, 1990.

[10] Spiteri, E. J. and Juanes, R.: 2004, Impact of Relative Permeability Hysteresis on the Numerical Simulation of WAG Injection, SPE 89921, in: Proceedings of SPE ATCE Houston, Texas.

[11] ECLIPSE 2007.2 Technical Description Manual. Hysteresis, Relative permeability hysteresis in the non-wetting phase.

[12] Jackson, D D, Andrews, G L, Claridge, E L, “Optimum WAG ratio Vs Rock wettability in CO_2 flooding”, SPE 14303, presented at 60th Annual technical conference and exhibition of the Society of Petroleum engineers held in Las Vegas, NV, Sept 22-25,1985.

[13] Shing-Ming C., Allard, D.R., and Anli, J.: .Factors Affecting Solvent Slug Size Hydrocarbon Miscible Flooding Requirements in Hydrocarbon Miscible Flooding,. SPE paper 12636 presented at the 4th Symposium on Enhanced Oil Recovery, Tulsa, OK,15-18, April.

[14] Gharbi-Ridha, B.C., .Integrated Reservoir Simulation Studies to Optimize Recovery from a Carbonate Reservoir,. paper SPE 80437 presented at the SPE Asia Pacific Oil and Gas Conference and Exhibition, Jakarta, Indonesia, 9-11 September.

[15] Green, D W, Willhite, G P, “Enhanced oil recovery”, SPE Textbook series, Volume 6, 1998.

[16] Yellig, W.F., Metcalfe, R.S., 1980. Determination and prediction of CO_2 minimum miscibility pressures. J. Pet. Technol. 1, 160–168.

[17] Merrill, R.C., Hartman, K.J. and Creek, J.L.: .A Comparison of Equation of State Tuning Methods, Paper SPE 28589 presented at the 69th Annual Technical and Exhibition New Orleans, LA, 25-28 September.

[18] Christie, M.A., and Blunt, M.: Tenth SPE comparative solution project: A comparison of Upscaling techniques. SPE 66599, Presented at the 2001 Reservoir Simulation Symposium, Houston, Texas, 11-14 February 2001.

[19] Web site for the 10th SPE Comparative Solution Project: **http://www.spe.org/csp/.**

[20] Petrel™ 2008.1 Reference Manual, Schlumberger.

[21] Chawathe, A., and Taggart, I.:" Insights Into Upscaling Using 3D Streamlines," Paper SPE 88846. Revised for publication from paper SPE 66379, first presented at the 2001 SPE Reservoir Simulation Symposium, Houston, 11–14 February.

[22] Kumar, A., C. L. Farmer, et al. (1997). Efficient Upscaling from Cores to Simulation Models (SPE Paper 38744). SPE Annual Technical Conference and Exhibition, San Antonio, Texas

APPENDIX A

The 10th comparative solution project

Description of the 10th SPE comparative Solution project Model:

The 2001 SPE Comparative Solution Project is the latest in a series of comparative solution projects organized by the Society of Petroleum Engineers.

The model has a simple geometry, with no top structure or faults. At the fine geological model scale, the model is described on a regular cartesian grid. The model dimensions are 1,200 x 2,200 x170 ft. The top 70 ft (35 layers) represent the Tarbert formation, and the bottom 100 ft (50 layers) represents Upper Ness.

The fine-scale cell size is 20 x 10 x2 ft. The fine scale model size is 60 x 220 x 85 cells (1.122x106 cells). [18]

Reservoir Model Description:

The model consists of part of a Brent sequence. The model was originally generated for use in the PUNQ project. The vertical permeability of the model was altered from the original. Originally, the model had a uniform Kv/K_h across the whole domain. The fine model has a Kv/K_h of 0.3 in the channels and a Kv/K_h of 10^{-3} in the background.

The top part of the model is a Tarbert formation, and is a representation of a prograding near shore environment. The lower part (Upper Ness) is fluvial. [18]

Well configuration:

All wells vertical and completed throughout formation.

Central Injector

4 producers

Downloadable files:

Download porosity and permeability file - por_perm_case2.zip (18.4MB) from the 10th comparative solution project, second data set. [19]

Table 5: Downloadable porosity and permeability files

Contains:	File 1:	Porosity (60 x 220 x 85)
	File 2:	K_x (i,j,k), i = 1,60, j = 1,220 k = 1,85
		K_y (i,j,k), i = 1,60, j = 1,220 k = 1,85
		K_z (i,j,k), i = 1,60, j = 1,220 k = 1,85

APPENDIX B:

Work flow of the model preparation

1- Model Building in Petrel™:

Building the model in Petrel consists of the following steps.

Step 1: Make Simple Grid

The Make Simple Grid process is located under Utilities, and provides a simple alternative to the pillar gridding process for creating 3D grids with no faults.[20]

This process is the first step in describing the model geometry and location. The thickness of the reservoir is 170 ft start at depth 12000 ft. In the make simple grid window the values (-12000) and (-12170) is assigned in top limit and bottom limit respectively.

The top and base of the 3D grid can be defined using constant values or surfaces. [20]

Model geometry in horizontal direction has to be specified in minimum and maximum values in feet.

$X_{minimum}$: 0 X_{max}: 1200

$Y_{minimum}$: 0 Y_{max}: 2200

The grid increment (cell dimension) was set to be 20 for X direction and 10 for Y direction.

Step 2: Make skeleton Grid

A ‘skeleton grid’ consists of a Top, mid, and bottom mesh defined by ‘pillars’ which define the lateral position of the corners in the three meshes, and the z-position is defined as the bottom, mid point, and the top of the pillars.

The ‘skeleton grid’ needs to be subdivided in the vertical direction by inserting surfaces. The highest and the bottommost surface that are inserted define the top and the bottom of the final 3D grid. Therefore, the top and the bottom ‘skeleton grid’ are usually outside the final 3D grid. Now the model should be converted to real grid using “convert to surface”.

Step 3: Make polygon

In this step a rectangular polygon, which is bottom Trabert, has to be created.

X origin = 0 Width = 1200 ft

Y origin = 0 Height = 2200 ft

Z value = - 12070 ft

Where 70 ft is the thickness of Tarbert formation

Step 3: Making Horizon

In order to define the vertical layering of the 3D grid in Petrel, we have to make horizon. The Make Horizons process step is the first step in defining the vertical layering of the 3D grid in Petrel.

This process usually defines the main depositional units of the 3D grid. Make Horizon samples input surfaces into the 3D Grid. Note that a 'Horizon' in Petrel is a surface that is a part of the 3D grid.[20]

In my case, we have three horizons, Top Tarbert, Bottom Tarbert, and Bottom Ness

Step 4: Making Zone

Zones are defined as the interval between two horizons. The Make Zones process is calculated one stratigraphical interval at a time. Each horizon delimits a stratigraphic interval. In my case, any two horizons will be considered as zone.

Step 5: Layering

Now the final vertical resolution of the 3D grid has to be assigned. In our case the model was assigned as 85 layers. The top 70 ft (35 layers) represent the Tarbert formation, and the bottom 100 ft (50 layers) represents Upper Ness.

Layering however, will not be defined by enclosing horizons. Layering is defined as the internal layering reflecting the geological deposition of a specific zone. They are only sub-dividing the grid between the zone-related horizons.[20]

In our model we used the option of "Building layering proportionally" which divides the zone into a given number of layers of the same thickness

2- Importing Grid Properties to the fine model:

Finally, it is possible to assign the grid properties to the fine model. The grid property data included in the 10th SPE example second dataset contains the porosity and the permeability in two downloadable files as follow.

File 1: Porosity (60 x 220 x 85)

File 2: Kx (i,j,k), i = 1-60, j = 1-220, k = 1,85

Ky (i,j,k), i = 1,60, j = 1-220, k = 1,85

Kz (i,j,k), i = 1,60, j = 1-220, k = 1,85

Figure 37 through 39 show the porosity and permeability for the fine model.

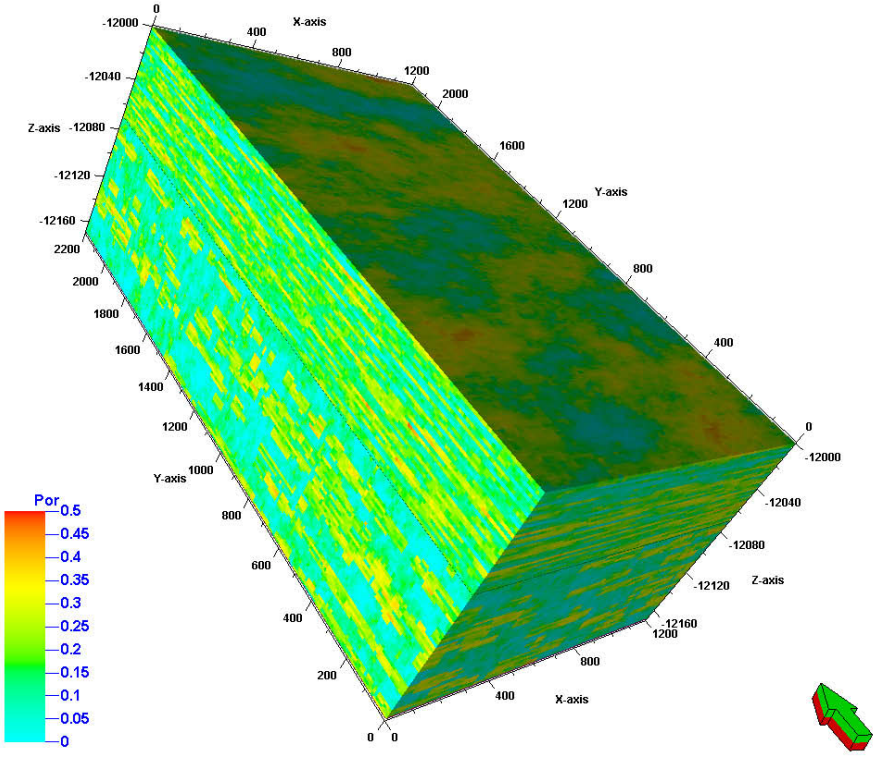

Figure 37: Fine model porosity.

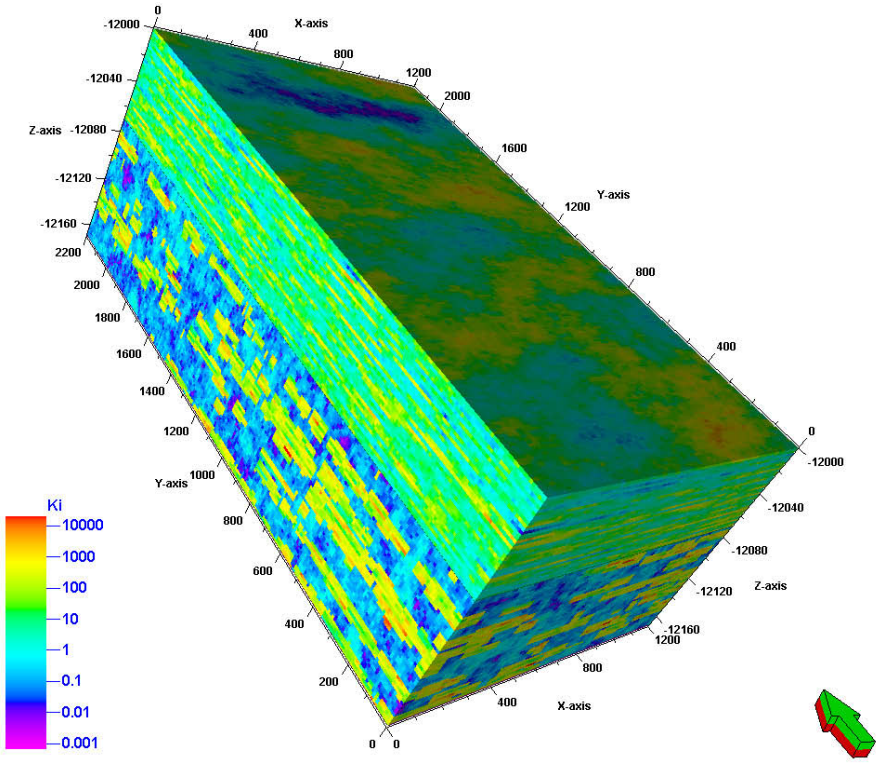

Figure 38: Fine model horizontal permeability.

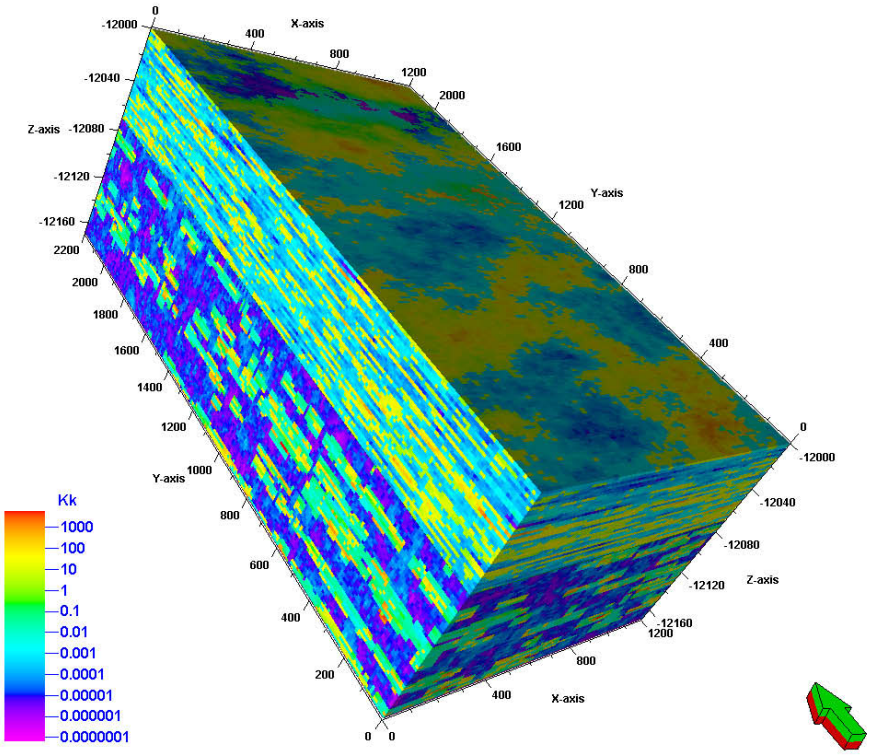

Figure 39: Fine model vertical permeability.

APPENDIX C:

Upscaling and exporting the model to ECLIPSE 300

Many reservoir flow simulators cannot directly and effectively handle the size of grids used in geological models. Such models can easily contain as many as 10 million cells, whereas single CPU simulations will only run in reasonable time with models of the order of 100,000 cells. Furthermore, grids used in geological models are often unsuitable for simulation due to geometric problems such as inside-out cells.[20]

Upscaling is the process of creating a coarser (lower resolution) grid based on the geological grid which is more appropriate for simulation. While this necessitates the omission of much of the geological models fine detail, the result is intended to preserve representative simulation behavior.[20]

Upscaling internally comprises two processes— up gridding, whereby the fine grid is optimally coarsened in such a way as to preserve the fractional-flow characteristics of the fine grid, and actual upscaling, whereby the effective properties for the coarsened grid are computed with established mathematical theories.[21]

Upscaling is necessary because important information about the reservoir is obtained on scales that are finer than the gridblocks of reservoir simulation.[22]

1- Upscaling

In Petrel, upscaling is split into three steps:

Creating the pillar grid for simulation:

Simulation grid (a coarser grid that will be used for flow simulation later) must be present in Petrel™ before the zones can be scaled up. The simulation grid is typically coarser than the geological grid and can be obtained by creating a new pillar grid from the existing fault model with a different grid size and generate the zones directly from the fine grid or by building a new, coarse grid in Petrel using Make Simple Grid and Scale up Structure. The geometry and faults of an existing fine grid are used as input.[20]

Choosing make simple grid is the start to describe the upscaled model geometry and location. The reservoir thickness is 170 ft start at depth 12000 ft. Values of (-12000) and (-12170) is assigned in top limit and bottom limit respectively using the geometry of the existing fine grid as input.

The geometry of the upscaled model in horizontal direction was specified as minimum and maximum values.

X minimum: 0 X max: 1200

Y minimum: 0 Y max: 2200

The grid increment for the upscaled model is the dimension of the cell and it was set to be 40 and 20 for both directions X and Y respectively.

Scale up Structure:

This process defines the new layering scheme (numbers and shapes of layers) of the simulation grid. In our case we kept the same numbers of layers for Tarbert and Ness. The top 70 ft (35 layers) represent the Tarbert formation, and the bottom 100 ft (50 layers) represents Upper Ness.

Subsequently, the upscaled model cell size is 40 x 20 x2 ft. and the model size is 30 x 110 x 85 cells (280,500 cells).

Scale up Properties:

This process populates grid properties, such as porosity and permeability, based on those in the fine grid.

Properties for our coarse grid can be derived from those in the fine grid by a variety of upscaling methods.[20]

Averaging methods was used for properties upscaling for two models.

Model 1: In this model arithmetic average has been chosen for porosity and permeability.

Model 2: In this model an arithmetic average for porosity and horizontal permeability and harmonic average for Vertical permeability.

By comparing the static properties, permeability and porosity distribution, the first model provided satisfactory results when compared with the fine model.

Figure 40 through 42 show the porosity and permeability for the upscaled model.

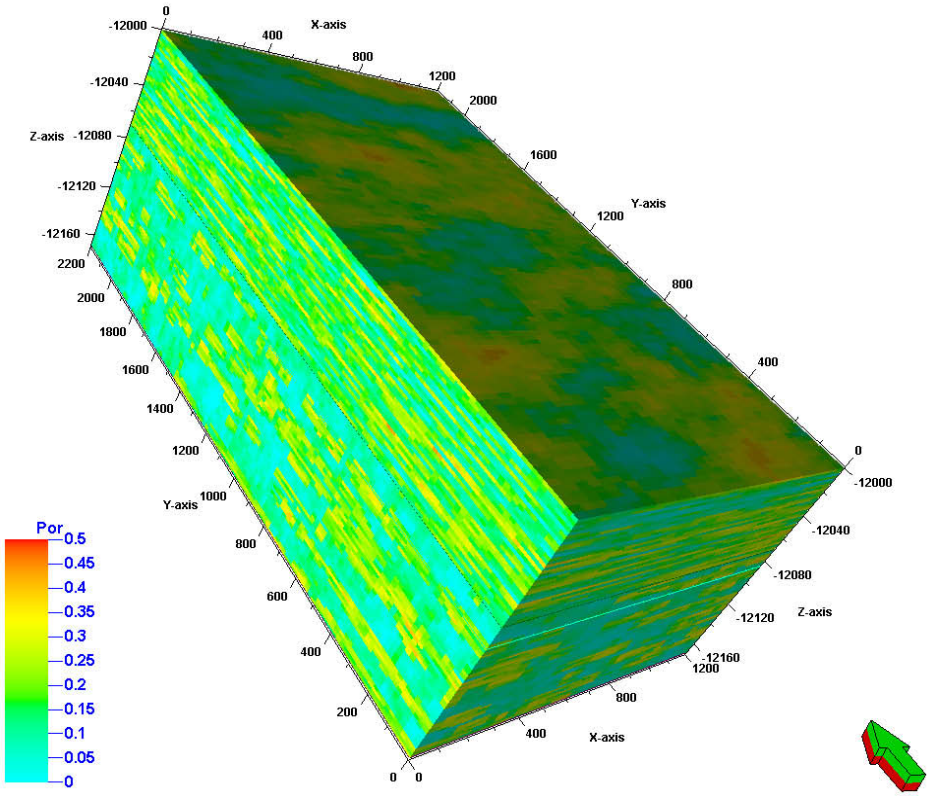

Figure 40: Upscaled model porosity.

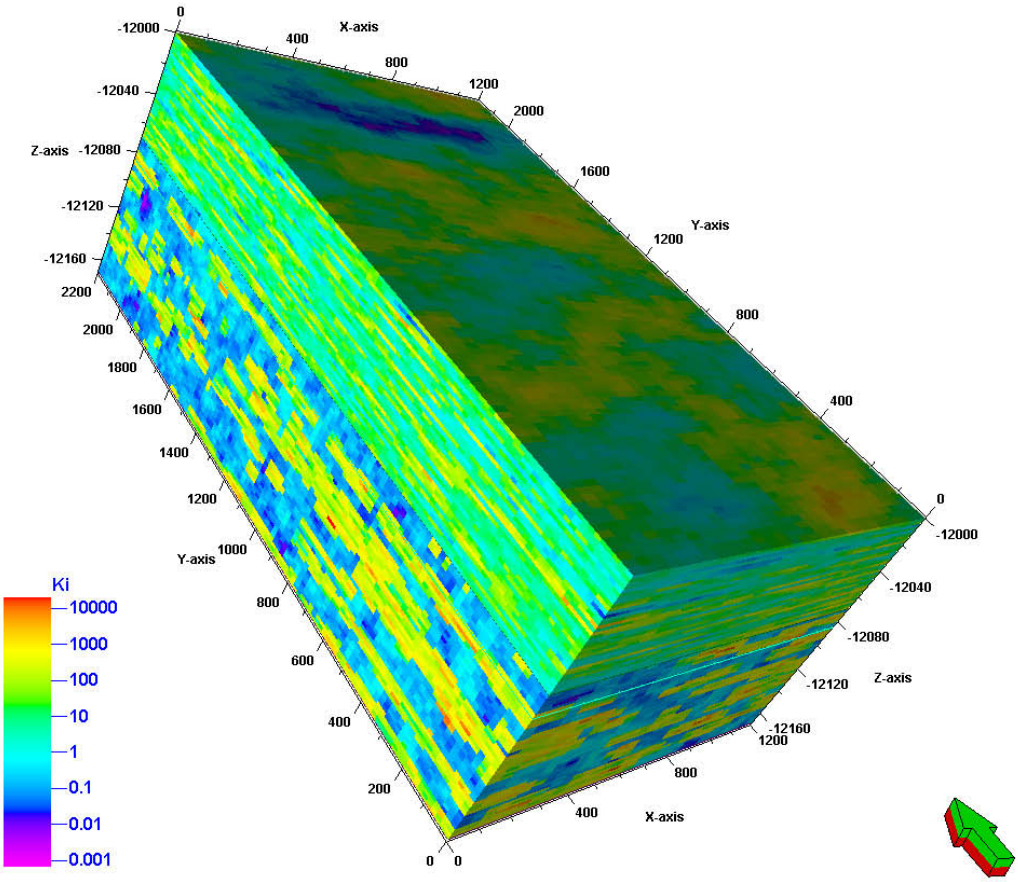

Figure 41: Upscaled model horizontal permeability.

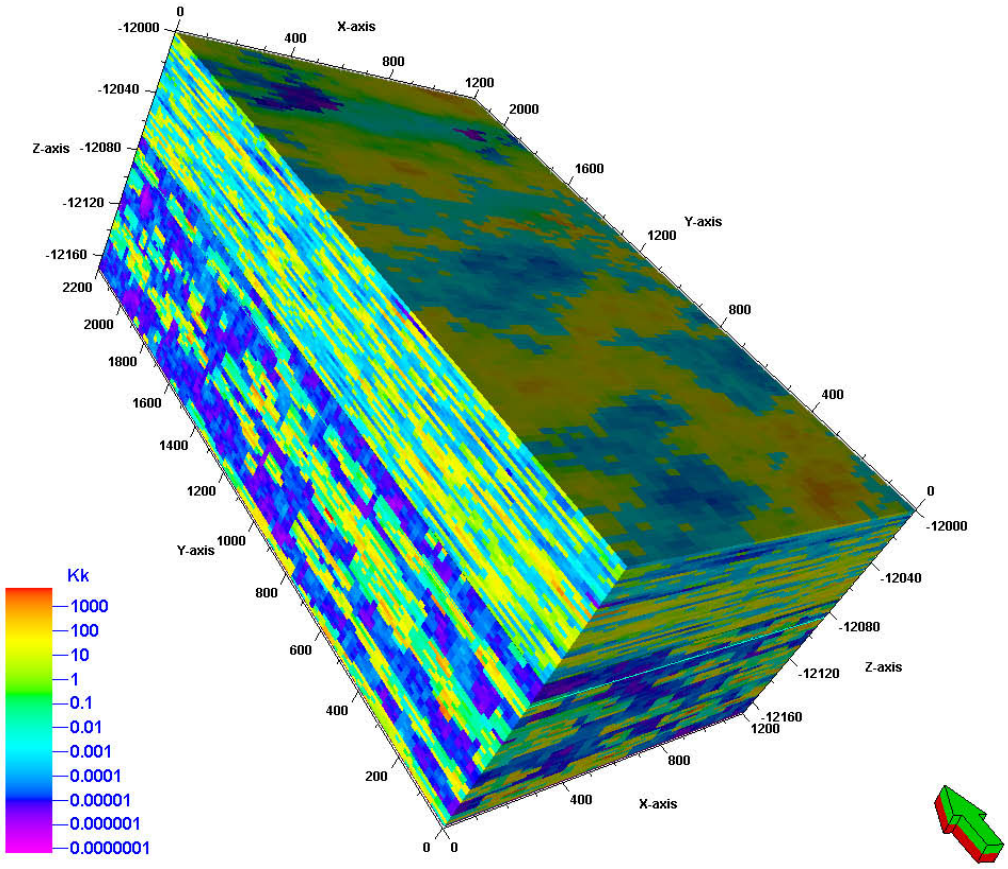

Figure 42: Upscaled model vertical permeability.

2- Exporting the Model to Eclipse:

Data from a Petrel geological model can be exported from Petrel to ECLIPSE. The output format needed for the dynamic simulation is *.GREDECL for the grid geometry and grid properties.

ECLIPSE Data File:

An ECLIPSE data input file is split into sections, each of which is introduced by a keyword.

The RUNSPEC section is the first section of an ECLIPSE data input file. It contains the run title, start date, units, various problem dimensions (numbers of blocks, wells, tables etc.).

The GRID section determines the basic geometry of the simulation grid and various rock properties (porosity, absolute permeability, net-to-gross ratios) in each grid cell. From this information, the program calculates the grid block pore volumes, mid-point depths and inter-block transmissibilities.

The PROPS section of the input data contains pressure and saturation dependent properties of the reservoir fluids and rocks. The SOLUTION section contains sufficient data to define the initial state (pressure, saturations, and compositions) of every grid block in the reservoir.

The SUMMARY section specifies a number of variables that are to be written to Summary files after each time step of the simulation. The graphics post-processor may be used to display the variation of variables in the Summary files with time and with each other.

The SCHEDULE section specifies the operations to be simulated (production and injection controls and constraints) and the times at which output reports are required.[20]

APPENDIX D:

WAG Calculation

CO_2 Compressibility and formation volume factor:

Reservoir pressure = 6000 psia
Reservoir Temperature = 200 ºF
CO_2 Critical Pressure = 1071 psia
CO_2 Critical Temperature = 87.91 ºF
Reduced Pressure, P_r = 5.60
Reduced Temperature, T_r = 1.20
Compressibility factor, Z = 0.76
Gas formation volume factor, B_g = 0.0004209 BBL/SCF

Volumes and Periods:

$$\text{Volume of } CO_2\text{, BBLs} = \text{HCPV} \times \text{Percent of } CO_2 \text{ Slug size}$$

$$\text{Period of } CO_2\text{, Months} = \frac{Volume\ of\ CO_2}{(Gas\ formation\ volume\ factor \times Gas\ injection\ rate \times 30.5)}$$

$$\text{Period of Water, Months} = \frac{Volume\ of\ Water}{(Water\ formation\ volum\ factor \times Water\ injection\ rate \times 30.5)}$$

Table 6: WAG calculation for 5 % HCPV CO_2 Slug size

	5 % HCPV CO_2 Slug size			
WAG Ratio	2 :1	1.25 :1	1 :1	0.5 :1
Volume of CO_2, BBLs	613659.8	613659.8	613659.8	613659.8
Volume of water, BBLs	1227319.6	767074.75	613659.8	306829.9
Period of CO_2, Months	15.9	15.9	15.9	15.9
Period of water, Months	8.0	5.0	4.0	2.0

CO_2 Injection rate = 3000M SCF/D, Water Injection rate = 5000 BBL/D

Table 7: WAG calculation for 10 % HCPV CO_2 Slug size

	10 % HCPV CO_2 Slug size			
WAG Ratio	2 :1	1.25 :1	1 :1	0.5 :1
Volume of CO_2, BBLs	1227319.6	1227319.6	1227319.6	1227319.6
Volume of water, BBLs	2454639.2	1534149.5	1227319.6	613659.8
Period of CO_2, Months	31.8	31.8	31.8	31.8
Period of water, Months	16.0	10.0	8.0	4.0

CO_2 Injection rate = 3000M SCF/D, Water Injection rate = 5000 BBL/D

Table 8: WAG calculation for 12.5 % HCPV CO_2 Slug size

	12.5 % HCPV CO_2 Slug size			
WAG Ratio	2 :1	1.25 :1	1 :1	0.5 :1
Volume of CO_2, BBLs	1534149.5	1534149.5	1534149.5	1534149.5
Volume of water, BBLs	3068299	1917686.87	1534149.5	767074.7
Period of CO_2, Months	39.8	39.8	39.8	39.8
Period of water, Months	20.1	12.5	10.0	5.0

CO_2 Injection rate = 3000M SCF/D, Water Injection rate = 5000 BBL/D

Table 9: WAG calculation for 15 % HCPV CO_2 Slug size

	15 % HCPV CO_2 Slug size			
WAG Ratio	2 :1	1.25 :1	1 :1	0.5 :1
Volume of CO_2, BBLs	1840979.4	1840979.4	1840979.4	1840979.4
Volume of water, BBLs	3681958.8	2301224.2	1840979.4	920489.7
Period of CO_2, Months	47.7	47.7	47.7	47.7
Period of water, Months	24.1	15.0	12.0	6.0

CO_2 Injection rate = 3000 M SCF/D, Water Injection rate = 5000 BBL/D

Table 10: WAG calculation for 12.5 % Slug size, 1:1 WAG ratio

	12.5 % Slug size , 1:1 WAG ratio			
WAG Ratio	2000	3000	4000	5000
Volume of CO_2, BBLs	1534149.5	1534149.5	1534149.5	1534149.5
Volume of water, BBLs	1534149.5	1534149.5	1534149.5	1534149.5
Period of CO_2, Months	59.79	39.8	29.9	23.9
Period of water, Months	10.1	10.1	10.1	10.1